Study of the Carbonized Plasma Facing Component and Its Application to the GAMMA 10 Tandem Mirror

Yuki ISHIMOTO

January 2003

Study of the Carbonized Plasma Facing Component and Its Application to the GAMMA 10 Tandem Mirror

Yuki ISHIMOTO

A dissertation submitted to the Doctoral Program
in Physics, the University of Tsukuba
in partial fulfillment of the requirements
for the degree of Doctor of Philosophy in Science

January 2003

Abstract

This thesis describes characteristics of the carbonized plasma facing component (PFC) and the application of the carbonized PFC to the GAMMA 10 tandem mirror.

Carbon sheet pump (CSP) is suitable to exhaust energetic hydrogen atoms under the condition of relatively low heat flux. The test module, in which a carbon sheet of 170 mm in diameter is mounted, is designed and fabricated in order to investigate the characteristics of pumping effect of CSP. It is confirmed from the pressure difference between CSP-on and -off that CSP has a pumping effect on the fast neutrals. In order to reduce the amount of the adsorbed gas molecule on the CSP surface, pumping experiments are conducted in the temperature range from RT to 250 ˚C. It is found that the amount of water molecule can be decreased by 70% compared with the case of RT. The analysis model on the basis of the pressure balance equation is proposed in order to estimate the pumping efficiency of CSP. The pumping efficiencies ξ of CSP are estimated to be 0.65 and 0.66 for the cases of 30 ˚C and 200 ˚C, respectively. There is no remarkable difference between two operational temperatures within the experimental error. The method, which reduces adsorbed gases on the CSP surface with sustaining a sufficient pumping efficiency, is established under the condition that CSP is used in actual plasma.

Samples of CSP have been analyzed by means of the Elastic Recoil Detection and the Rutherford Backscattering Spectroscopy techniques for the sake of improvement of CSP performance. It has been confirmed that fast neutrals emitted from an actual plasma are trapped in CSP by comparing the hydrogen depth profile of fast neutrals to that of the annealed sample. The hydrogen depth profile caused by fast neutrals has been roughly explained from the result of Maxwell-distributed ion irradiation by use of

the Monte Carlo simulation code TRIM.

CSP is newly applied to the shine-through beam dump of the neutral beam injector in order to examine the pumping characteristic of CSP under the condition of high heat and particle load. The result of heat transfer calculation shows that CSP can be used under the present experimental condition by the use of high heat conductive materials. The CSP beam dump is produced on the basis of the thermal design. The number of particles trapped by CSP is proportional to that of incident ones in the pumping experiment. It is confirmed that the pumping efficiency is improved to be 0.82 by adjusting the regeneration temperature to 750 ˚C. It is also found that the recovery of pumping efficiency by regeneration.

In order to consider whether the application of CSP can suppress the hydrogen recycling enhanced by neutral beam injection, the pumping effect of CSP on the GAMMA10 plasma is predicted by means of numerical simulation. A zero-dimensional particle and power balance model in the central cell is proposed. The model can qualitatively explain the present neutral beam injection experiment. The coverage of CSP is estimated to be 37 % of the inner wall area of the mid-plane. The increment of the neutral density after neutral beam injection is drastically reduced and the comparison between with and without CSP indicates the possibility that CSP can improve the energy and particle confinement in neutral beam injection experiments.

Contents

1. Introduction

It is widely recognized that reduction of hydrogen recycling is one of the important subjects for improvement of the plasma performance in the present fusion devices [1]. Hydrogen molecules and/or atoms adsorbed on the inner wall and limiters *etc*. are desorbed by incident ions, electrons and charge exchange fast neutrals emitted from plasma. The desorbed hydrogen goes back to plasma. This phenomenon is known as hydrogen recycling. The drop of energy confinement time is occurred owing to the increase of charge exchange loss induced due to the rise of neutral density [2]. In addition, it is impossible to control the plasma density when recycling coefficient exceeds unity. Therefore hydrogen recycling is also an important issue from the viewpoint of plasma control.

Fuel particles of plasma are supplied not only by gas puffers, cryogenic pellets [3] and neutral beam injection (NBI) [4-6] but also by hydrogen recycling. Gas puffers, cryogenic pellets and NBI are controllable, while hydrogen recycling is difficult to control because hydrogen recycling depends on the material of the first wall and the history of particle bombardment, temperature and gas pressure. Hydrogen recycling depends on the condition of inner wall such as surface density of hydrogen and the particle flux. To improve the former, baking and some kinds of discharge cleaning have been performed in many devices [1, 7-11]. Concerning the latter, the region of plasma surface interactions (PSI) is separated from the main plasma by magnetic divertor *etc*. [12, 13]

GAMMA 10 is a minimum-B anchored tandem mirror with thermal barrier [14]. The PSI studies of GAMMA 10 have two aspects. One is reduction of hydrogen

recycling; the other is suppression of impurities. In addition to be mentioned in the above paragraph, low temperature ions are trapped by thermal barrier potential, which makes the potential shallow. Bremsstrahlung caused by existence of impurities lowers electron temperature, which reduces the plug potential for ion confinement. Thus PSI in GAMMA 10 have a deep connection to potential formation. It is thought that the problem of impurity in the plug cell is not serious because the effective charge of the central cell plasma is evaluated to be 1.0 from the VUV spectroscopy [15]. Low temperature ions are exhaust by the mechanism called 'natural pumping' in the barrier cell. Therefore it is considered that the reduction of hydrogen recycling in the central cell is the most important in PSI issues of the present GAMMA 10.

In March 2001, a new neutral beam injector was installed in the central cell [6]. The objective of this neutral beam injector is to supply hot ions to main plasma and heating. Hα intensity is increased during NBI and it is considered to be caused by enhancement of hydrogen recycling since the rate coefficient of charge exchange reaction is much larger than those of proton and electron ionization in the present plasma parameter. The diamagnetism of the plasma decreases when the electron density slightly increases. This suggests the decrease of ion temperature. Hence to reduce hydrogen recycling during NBI is an issue to be solved.

In fusion devices, the discharge cleaning is carried out before main discharge in order to remove the hydrogen and impurities. Hydrogen can be trapped by the first wall during main discharges, which is called wall pumping [8, 16, 17]. The wall pumping has an important role in reduction of hydrogen recycling, the lifetime of the wall pumping is too short for applying long pulse experiments because discharge cleaning such as helium glow discharge cleaning cannot remove sufficient hydrogen in the first wall. It is reported that the Hα emission and the neutral pressure had only 5-8 shot e-hold for neutral beam heated discharges [1].

The carbon sheet pump (CSP) [18, 19], which was developed for pumping in the divertor region of Large Helical Device (LHD), is suitable to exhaust energetic hydrogen atoms under the condition of relatively low heat flux. The small-scale test module of CSP was designed in order to examine pumping characteristics in GAMMA 10 [20]. Because almost all trapped particles in CSP are desorbed by the regeneration phase in which CSP is heated up to approximately 700 ˚C for tens of minutes, CSP has longer lifetime than that obtained by discharge cleaning.

So far, the pumping effect of CSP on fast neutrals has been confirmed by macroscopic quantities such as hydrogen pressure in the test chamber [20, 21]. Samples of CSP exposed to fast neutrals must be analyzed by using microscopic techniques in order to improve the performance of CSP and to examine the applicability of CSP to actual devices [22]. It has been considered that CSP is applied under low heat flux since a high temperature leads to decrease of a total amount of hydrogen retention in carbon materials [23-25] and increase of the chemical sputtering yield [26-28]. However, heat and particle load to the first wall has a tendency to increase with improvement of plasma performance and extended pulse length. Therefore, in order to study the capability of CSP under high heat flux circumstance, CSP is newly installed to the shine-through beam dump of the neutral beam injector (CSPBD) [29]. In order to examine whether the application of CSP can suppress the hydrogen recycling enhanced by NBI, the effect of CSP on the GAMMA 10 plasmas is predicted on the basis of particle and power balance equations in the case where CSP is applied to the central cell.

The contents of this thesis are as follows: experimental apparatus are described in chapter 2. The pumping principle and the effect of CSP in the test module is presented in chapter 3. The analysis of carbon materials exposed to the GAMMA 10 plasmas is described in chapter 4. CSP beam dump, an application of CSP to GAMMA 10, is

shown in chapter 5. The calculation of time evolution of plasma parameter on the basis of particle and power balance is explained in chapter 6. Finally, the conclusion obtained in this thesis is described in chapter 7.

2. Experimental Setup

2.1 GAMMA 10 tandem mirror

2.1.1 GAMMA 10 device

GAMMA 10 is a minimum-B anchored tandem mirror with thermal barrier. Figure 2-1 shows the coil arrangement, the magnetic flux tube, the location of heating system and magnetic field strength on the machine axis of GAMMA 10. In the figure, the z-axis is defined as the machine axis and the positive direction of the z-axis corresponds to the direction of magnetic line of force on the axis. Other axes are shown in Fig. 2-2. The GAMMA 10 device consists of axisymmetric central cell, two anchor cells with minimum-B configuration located in both end of the central cell, two plug/barrier cells are located outside of each anchor cell. Main plasma is confined in the central cell. The plasma in the anchor cell assures MHD stability to the whole GAMMA 10 plasma. The GAMMA 10 plasma between both plug/barrier cells is confined electrostatically by plug potential generated by electron cyclotron resonance heating (ECRH). The electric power to GAMMA 10 is supplied by 250 MVA motor generator. The interval between plasma shots limited by cooling of magnetic coils is usually 12 minutes.

2.1.2 Pumping system

As shown in Fig. 2-2, there are three kinds of pumping systems in GAMMA 10 in order to maintain good vacuum condition. Six turbo molecular pumps (TMP) are mounted in the central, the anchor and the end cells. The pumping speed of TMP is 3 m^3/s for hydrogen molecule. Ten cryosorption pumps (CP) are attached to barrier cells, the central cell and dump tanks. The pumping speed of CP in the central cell is 10 m^3/s,

others are 18 m^3/s for hydrogen molecule. Large-scale liquid helium cryopanels (LHP) are mounted on the top of the east and the west mirror tanks and injection tanks of the anchor neutral beam injector [30]. LHP is cooled down to 3.5 K and gas molecules are condensed on the panel without catalysts. The total amount of pumping speed of LHP is designed to be 2600 m^3/s. Base pressure is sustained of the order of 10^{-5} Pa in the central cell.

2.1.3 Heating and fueling systems

• Neutral beam injector

There are 4 NBI systems (7 units) in GAMMA 10. Sloshing NBI (S-NBI) system and Pumping NBI (P-NBI) system inject neutral beams into the mid-plane of the both plug/barrier cells. S-NBI system generates sloshing ion distribution for potential formation. P-NBI system is used so as to exhaust cold ion trapped in thermal barrier. The difference between these two NBI systems is incident angle with respect to the z-axis. Energetic particles generated by S-NBI and P-NBI systems are incident to inside and outside of loss cone, respectively. Anchor NBI (A-NBI) system sustains high-beta plasma in the cell for MHD stability by the ion heating and fueling ions. The angle between the z-axis and the beam line of A-NBI is 82˚. The maximum power of the ion sources of above NBI are 25 kV and 70 A (1.75 MW, 0.1sec) per one unit.

In March 2001, a new neutral beam injector was installed in the central cell (C-NBI system) [6]. The objective of C-NBI is to supply the energetic particle to main plasma and plasma heating. The beam line of C-NBI is perpendicular to the plasma column and is 2 cm below z-axis taking account of the Larmor radius of the trapped ion. The maximum power of the ion source of C-NBI is 25 kV and 30 A (0.75 MW, 0.1sec). The divergence angle of total beam is 1.3˚ and neutralizing efficiency is estimated to be 72 % from the measurement with arrays of beam attenuation detectors (BAD) and

calorie meters (CM).

• Ion cyclotron range of frequency heating (ICRF)

The plasma sustained by ICRF system and gas puffing is generated by plasma guns located at both ends. The power of ICRF1 (ω ~10 MHz, 500 kW, 0.5 sec) supplied to Nagoya type III antennas excites fast wave and ions in the anchor and the central cells are heated. ICRF2 (ω ~ 6.36 MHz, 500 kW, 0.5 sec) excites slow wave by means of Double Half Turn antenna and is used for heating of ions in the central cell. New ICRF system (ICRF3, ω/ω_{ci} ~ 10, 100 kW, 0.5 sec) was installed in order to plasma production. The power of ICRF3 is supplied to the Double Half Turn antenna mounted in the west inside of the central cell.

• Electron cyclotron resonance heating (ECRH)

In order to heat electrons, four ECRH systems with 28 GHz gyrotron (200 kW, ~0.1 sec) are applied. The microwave for barrier potential (for electron confinement) is incident on the mid-plane of plug/barrier cell in which magnetic field strength is ~0.5T. The plug potential for ion confinement is formed by the plug ECRH near the fundamental cyclotron resonance surface of 1T. Both plug potentials are formed at the outside of the mid-plane.

• Fueling system

For plasma sustenance and density control, gas puffing (GP) systems are mounted at various locations in GAMMA 10. The gas puffing system used in recent experiments is described here. The locations of GPs are shown in Fig. 2-2. GP#1b and GP#2b are used to start up the plasma by injecting dense gas with a duration of ~0.02 sec. The piezoelectric valves of GP#1b and GP#2b are located in the vacuum vessel for fast

response. GP#3 and GP#4 located at the mirror throat of the central cell are applied to sustain plasma. The piezoelectric valves of GP#3 and GP#4 are connected to gas rings surrounding the plasma for uniform fueling. GP#7 located at the mid-plane of the central cell is used during electron cyclotron resonance discharge cleaning (ECRDC) carried out for ~24 hours before main discharges [11].

2.1.4 Diagnostic system

• Microwave interferometer [31]

The electron line density of plasma is measured with microwave interferometer. The line density is evaluated by phase difference between plasma and reference arms. The interferometer mounted on the mid-plane of the central cell can scan along the y-direction. The radial profile of electron density can be reconstructed by applying the Abel inversion.

• Diamagnetic loop [31]

Plasma pressure perpendicular to the magnetic field is evaluated from the decrement of the field caused by the plasma diamagnetism. The pressure is proportional to the product of ion and electron temperature (T_i and T_e) and plasma density. The plasma diamagnetism is proportional to the product of T_i and electron density because T_i is much higher than T_e in the hot-ion mode plasma. Therefore, the ion temperature averaged in the inside of the loop can be estimated if the density is given.

• Charge exchange neutral particle analyzer (CX-NPA) [32, 33]

Charge exchange fast neutrals have information of ion temperature in the plasma. Fast neutrals emitted from the plasma lose their electrons in the stripping cell. The stripped ion is obliquely incident into the parallel electrode energy analyzer. Ion

temperature is estimated from measured energy spectrum. Since the mean free paths of the charge exchange reaction and the ionization processes of fast neutrals are much longer than the plasma diameter (~0.4 m) in the central cell, the radial profile of ion temperature is obtained by scanning line of sight.

• Fast ionization gauge

Nude-type Bayard-Alpert gauge (NG) is adopted to measure the hydrogen pressure during plasma discharge for fast response and higher sensitivity than triode type gauge. NG equipped with magnetic shield is installed in each cell.

2.2 Carbon Sheet Pump

2.2.1 Test module

The CSP test module for evaluation of the pumping characteristics is located in the central cell of GAMMA 10. Figure 2-3 shows the schematic view of the CSP test module [20, 21]. The module can be water-cooled as necessary. CSP is made of a two-dimensional C/C sheet (CX-270, Toyo Tanso) of 0.15 cm thickness with a diameter of 17 cm. CSP can be heated by direct joule heating (~60 V, ~30 A) up to about 800 °C. In front of the CSP, a rotational shutter is mounted in order to intercept the incident charge exchange fast neutrals and the pumping effect is examined by using the shutter (CSP-on and CSP-off) shot by shot. It was confirmed that the difference of conductance between CSP-on and CSP-off is negligible. NG with magnetic shield is installed into the module. Total pressure in the module is measured by this NG. Impurity gases are measured during plasma discharges and in thermal desorption experiments with quadrupole mass spectrometer (QMS). Temperatures of carbon sheet and several locations of the module are measured with chromel-alumel thermocouples (TC).

2.2.2 Surface station and surface analysis system

The surface station to expose samples to fast neutrals is installed to the test module as shown in Fig. 2-3. Charge exchange fast neutrals with relativity high energy (0.5~5 keV) are in this cell. Samples exposed to fast neutrals are the C/C material used as CSP in our test module and their size is 20 x 10 x 1.5 mm^3. The samples are annealed at a temperature of 800 ˚C for 10 minutes before the exposure. They are analyzed by means of elastic recoil detection (ERD) [51] and Rutherford backscattering spectroscopy (RBS) techniques [51] using a several MeV helium ion beam in the laboratory of Prof. Morita in Nagoya University [25]. Figure 2-4 shows the schematic illustration of the surface analysis system in the laboratory. Helium ion beam extracted from Van de Graff accelerator is incident in the analysis chamber and the sample can be analyzed by ERD and RBS techniques simultaneously. The depth profile of hydrogen density is measured with the ERD technique. Elements in near-surface region can be identified by the RBS. The objective of RBS is to investigate the existence of impurity from plasma. The detail of these two methods is described in chapter 4.

2.2.3 CSP beam dump

As mentioned above, the C-NBI system was recently installed in the central cell for plasma heating and fueling. Due to the low line density of the present GAMMA 10 plasma (~5 x 10^{13} cm^{-2}, T_e = ~ 80 eV), about 95 % of incident neutral beam passes through the plasma column [53]. The large amount of gaseous hydrogen caused by shine-through beam causes high pressure in the dump tank. The purpose of CSP beam dump (CSPBD) is not only to examine the pumping effect under the condition of high heat and particle load but also to reduce the backward flow gas to the central cell by pumping. Figure 2-5 shows a cross sectional schematic of C-NBI system.

A photograph of CSPBD produced on the basis of the thermal design is shown in Fig. 2-6. The details of thermal design are described in chapter 5. CSPBD consists of 50 strips of C/C sheet of 11 mm in width and 1.5 mm in thickness, the length of which changes the various sizes (250~400 mm) depending on the location. The strips incline at 60 degrees to the incident beam in order to reduce the heat flux density. Each strip is electrically connected in series and CSPBD is heated up to ~700 ˚C in the regeneration phase. In front of CSPBD, a rotational stainless shutter which intercepts neutral beam (NB) is mounted. The pumping capability of CSP can be examined by the use of this shutter (CSP-on and CSP-off). The flux at the beam center of NB (2.5 x 10^{21} H/m^2 s) is approximately one thousand times larger than that of fast neutrals emitted from the GAMMA 10 plasma (~10^{18} H/m^2 s). This enables to examine the pumping effect of CSP in the high flux circumstance. The pressure rise caused by NB is measured with a fast ionization gauge.

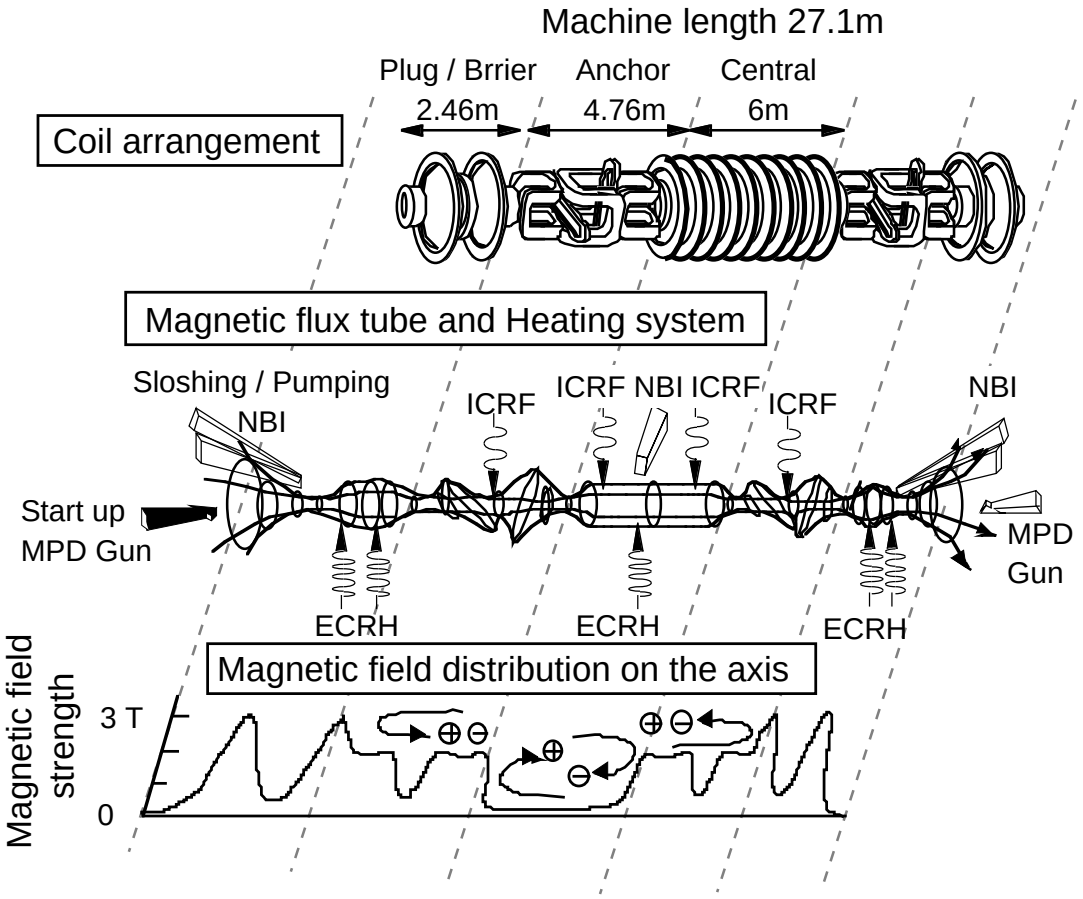

Fig. 2-1 (a) Coil arrangement, (b) a shape of magnetic flux tube and (C) magnetic field strength of the GAMMA 10 tandem mirror.

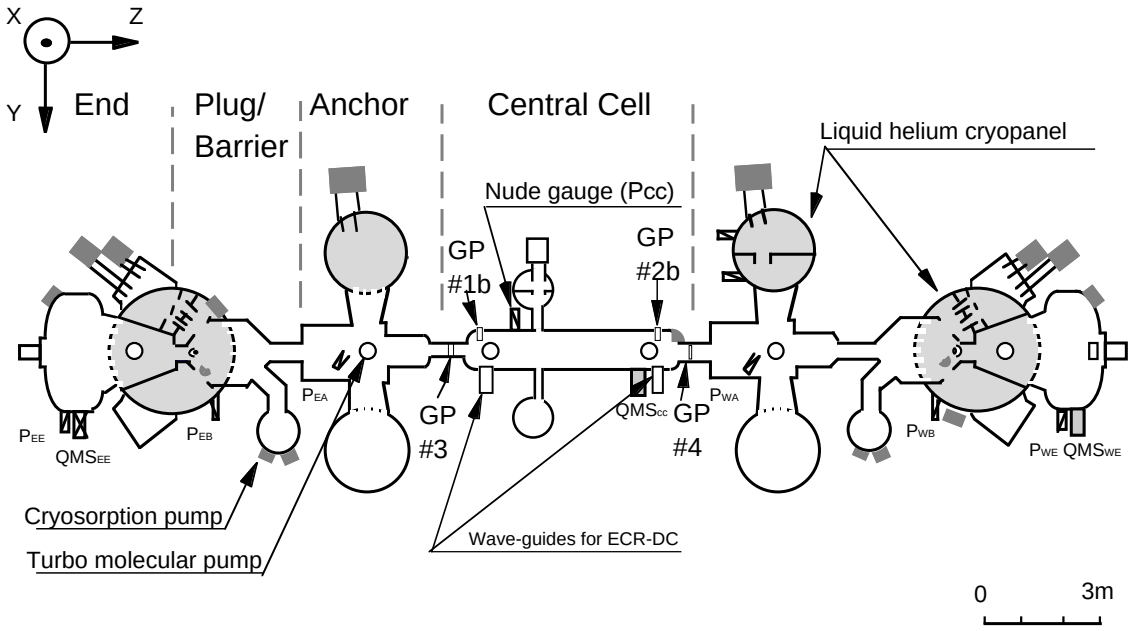

Fig. 2-2 A schematic of the vacuum vessel and the location of the pumping and the fueling system of GAMMA10.

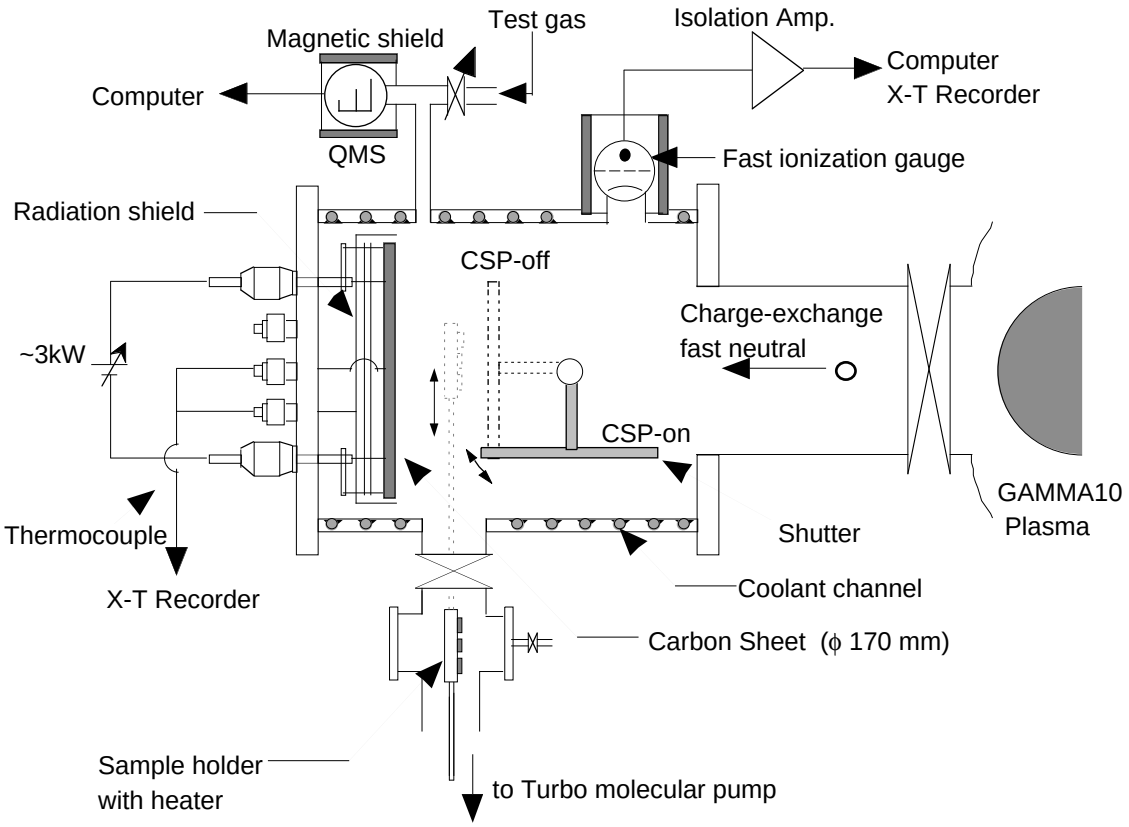

Fig. 2-3 Schematic view of the CSP test module.

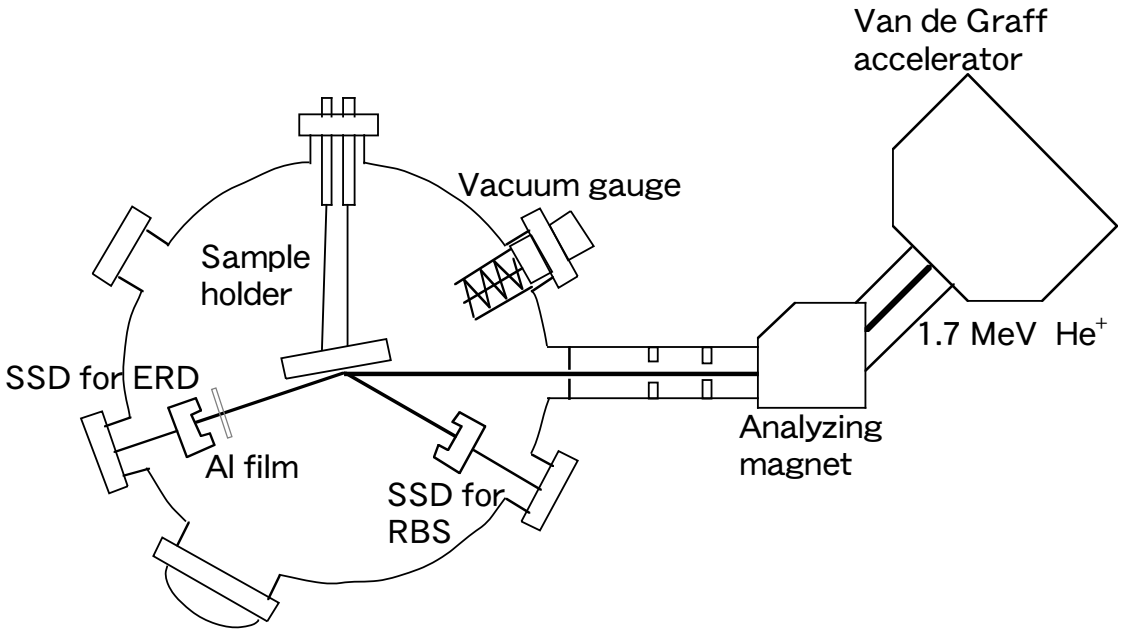

Fig. 2-4 Schematic illustration of the surface analysis system in the laboratory of Prof. Morita in Nagoya University.

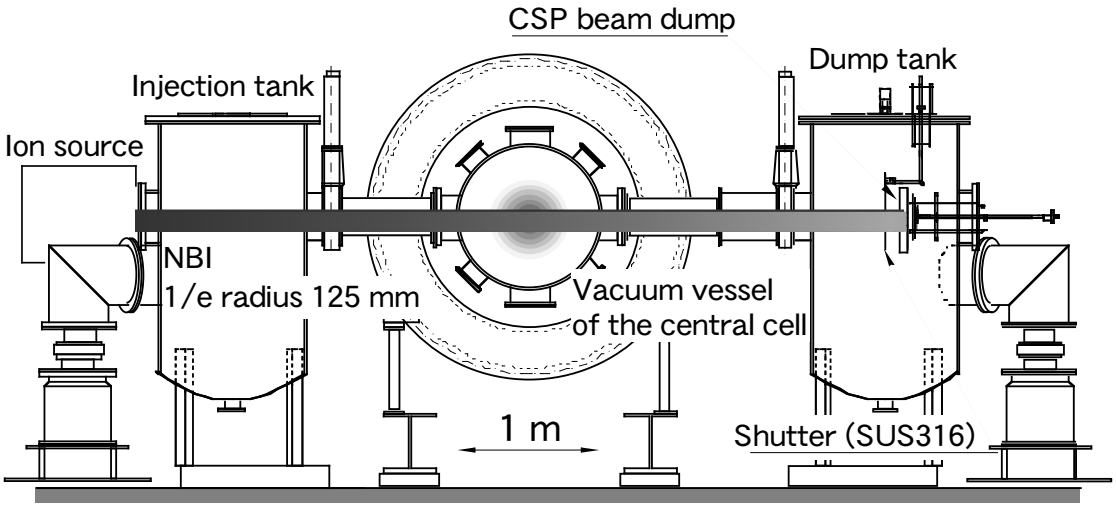

Fig. 2-5 A cross sectional schematic of C-NBI system.

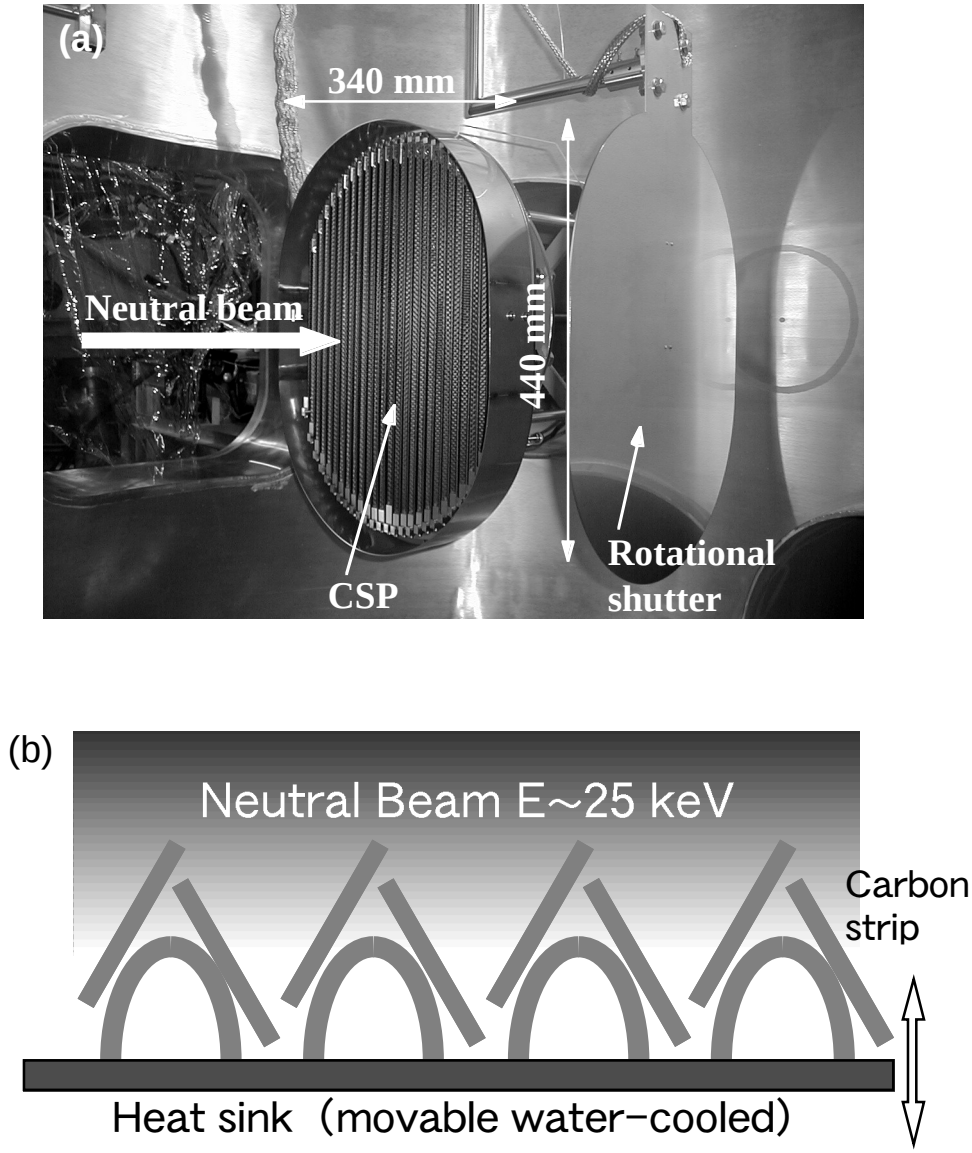

Fig. 2-6 (a) A photograph of CSP beam dump. (b) A schematic cross sectional view of CSPBD.

3. Pumping characteristics of the Carbon Sheet Pump in the test module

3.1 Carbon sheet pump

3.1.1 Pumping principle of CSP

In carbon material, almost all incident particles are trapped due to the low reflection coefficient for energetic particles. CSP can pump out fast neutrals emitted from hot-ion mode plasmas by this phenomenon. Particle reflection coefficient in the case of normal incidence R_N is given by [34, 35],

$$R_N(\varepsilon) = \left[\left(1 + 3.2116\varepsilon^{0.34334}\right)^{1.5} + \left(1.3288\varepsilon^{1.5}\right)^{1.5}\right]^{-2/3}, \tag{3-1}$$

$$\varepsilon = 32.55\frac{M_2}{M_1 + M_2}\frac{E_i}{Z_1 Z_2\sqrt{Z_1^{2/3} + Z_2^{2/3}}}, \tag{3-2}$$

where E_i is incident energy of particle (keV), ε is the reduced energy. Z_1, M_1 and Z_2, M_2 are the atomic number and mass of incident particle and target atom, respectively. The reflection coefficient for actual plasmas $\overline{R}_N$ is estimated from the integral of Eq. (3-1) multiplied by Maxwell distribution, $f(T_i, E)$,

$$\overline{R}_N(T_i) = \frac{\int R_N(E) f(T_i, E) dE}{\int f(T_i, E) dE}. \tag{3-3}$$

The particle reflection coefficients for single energy and Maxwell-distributed particles are shown in Fig. 3-1. Each coefficient decreases with increase of energy or ion temperature. Almost all incident particles emitted from hot-ion mode plasmas can be trapped in the carbon material (*e.g.* When ion temperature is 5 keV, $\overline{R}_N$ is estimated to be 0.04. Accordingly ideal pumping efficiency is deduced to be 96%.)

3.1.2 Regeneration cycle of CSP

The amount of hydrogen in carbon material increases with the incident energy because the projected range of the incident particle increase with its energy. Carbon material can continuously trap hydrogen atoms until the saturated concentration of H/C reaches ~0.4 [36, 37]. The empirical formula of saturation amount in deuterium bombardment experiment is given by Staudenmaier et al. [36],

$$F_{sat} = 3.5 \times 10^{18} E^{0.9} \text{ for carbon} \quad (50 < E < 20\ 10^3 \text{ eV}), \tag{3-4}$$

$$F_{sat} = 3.5 \times 10^{18} E^{0.8} \text{ for silicon} \quad (50 < E < 1\ 10^3 \text{ eV}), \tag{3-5}$$

where F_{sat} is saturation amount of deuterium (D/m^2). E is incident energy (eV). Although saturated carbon material does not have pumping capability any longer, it is confirmed that most of trapped hydrogen can be desorbed by heating it up to 700 ˚C for ~30 minutes [18]. Thus it is considered that CSP can be used repetitiously. The degassing is called regeneration or thermal desorption experiment [38, 39]. The operation of CSP repeats the pumping and the regeneration phases alternately.

From Eq. (3-4), the saturation amount of CSP for the GAMMA 10 plasma is roughly estimated to be 7 x 10^{21} D/m^2. It is assumed that the typical ion temperature is ~5 keV. The charge exchange fast neutral flux Γ_{CX} is given by

$$\Gamma_{CX} = n_i n_0 \langle \sigma v \rangle_{cx} V_{plasma} / S_{wall}, \tag{3-6}$$

where n_i and n_0 are ion and neutral density, respectively. $\langle \sigma v \rangle_{cx}$ is the rate coefficient of charge exchange taking Maxwell distribution of ions into consideration. V_{plasma} and S_{wall} are the effective volume of plasma and the effective area of the inner wall of the central cell, respectively. Γ_{CX} is estimated to be 1.4 x 10^{18} H/m^2 s by substituting typical plasma parameters into Eq. (3-6) [21]. Therefore, the regeneration cycle of CSP is calculated to be ~5000 seconds when the cycle is defined as F_{sat} / Γ_{CX}.

3.1.3 Trapping state of hydrogen in carbon material

It is considered that there are two hydrogen trapping site in carbon materials. One is the C-H bond (~4 eV) which is confirmed from the SIMS measurement [40]. The deep trap (lattice defect) is caused by the displacement of carbon atom by the collision cascade (damage) and distortion of the crystal due to the fabrication (nature). The other is the shallow trap proposed by Morita [25, 41] and Brice [42]. It is supposed that the hydrogen is weakly bound to the carbon atom. The experimental results carried out under different conditions are well explained by the introduction of the shallow trap.

The mass-balance equations proposed by Morita are described here because the detailed processes of the hydrogen transport are taken into account. In the mass-balance equations, hydrogen atoms are divided into two groups (*i.e.* trap and mobile). The equations are expressed as follows:

$$\frac{dn_M(x,t)}{dt} = D\frac{\partial^2 n_M(x,t)}{\partial x^2} + v_{rec}\frac{\partial n_M(x,t)}{\partial x} - \Sigma_T n_M(x,t)\left[C_0 - n_T(x,t)\right]$$

$$+n_T(x,t)\left(\Sigma_d + \sigma_T\phi\right) - Kn_T(x,t)n_M(x,t) - 2K_1 n_M(x,t)^2 + \phi f(x), \quad (3\text{-}6)$$

$$\frac{dn_T(x,t)}{dt} = v_{rec}\frac{\partial n_T(x,t)}{\partial x} + \Sigma_T n_M(x,t)\left[C_0 - n_T(x,t)\right]$$

$$-n_T(x,t)\left(\Sigma_d + \sigma_T\phi\right) - Kn_T(x,t)n_M(x,t), \quad (3\text{-}7)$$

where $n_M(x,t)$ and $n_T(x,t)$ are the mobile and the trap hydrogen density, respectively, v_{rec} is the recession velocity of surface, C_0 is the trap density, ϕ is the particle flux, $f(x)$ is the normalized projected range of incident particles. Σ_T, Σ_d and K denote rate constants of trapping, thermal detrapping and the local molecular recombination [43, 44] between the mobile and the trap hydrogen. K_1 is the rate coefficient of the local molecular recombination between mobile hydrogens. σ_T is the cross section of ion-induced detrapping [45].

Figure 3-2 shows the schematic diagram of the hydrogen transport in the carbon

material proposed by Morita. The activation energies presented in the figure are evaluated by use of these equations under the various experimental procedures [25, 41].

3.2 Pumping effect of CSP during plasma discharges

Figure 3-3 shows the time evolution of hydrogen pressure in the test module and the central cell during plasma discharges. The pressure difference is occurred only in the test module. The module is too small to have an influence on the pressure in the central cell. The time evolution of plasma parameters (*e.g.* electron line density, diamagnetism and Hα line intensity) is also the same in these cases. Therefore, the pressure difference between CSP-on and off is caused by reduction of hydrogen recycling in the module. This result indicates the pumping effect of CSP on fast neutrals.

Figure 3-4 shows the time evolution of hydrogen pressure in the module during plasma discharges under various heating power of ICRF2. Pressure differences between CSP-on and -off increase with the heating power. It is also confirmed by CXNPA that the flux of fast neural increases with the heating power. Hence the number of trapped particle by CSP increases with that of incident one.

3.3 Reduction of adsorbed gas on the CSP surface

Even in the CSP-off experiment, considerably large pressure rise is observed during the thermal desorption experiment. The experiments results suggest that the carbon sheet not only traps fast neutrals but also adsorbs the gases such as hydrogen and water molecules to a certain extent on the surface under the operation in the actual plasma devices. Adsorbed gas molecules on the surface must be reduced because the molecules induce hydrogen recycling and/or impurity generation.

In general, there are two ways to reduce the adsorbed gas on the surface. One is

reduction of pressure in the vessel; the other is to heat up the vessel. The former is difficult to perform because the hydrogen pressure is strongly related with plasma parameters. The latter way is adopted and a series of experiments is carried out in which the carbon sheet is exposed to fast neutrals at various temperatures from RT to 250 ˚C.

It is reported that a high temperature of carbon material reduces the total amount of trapped particles [23-25]. We investigated the pumping effect of CSP with an operational temperature of 200 °C. Figure 3-5 shows the time evolutions of total pressures in the test module (P_{CSP}) and GAMMA 10 (P_{CC}). The pressure difference occurs in the test module as same as the experiments of room temperature. This result indicates pumping effect of CSP at the operational temperature of 200 °C.

Figure 3-6 shows the results of thermal desorption experiments after exposure of CSP to charge exchange fast neutrals (CSP-on) with the operational temperature of 30 ˚C and 200 ˚C. In each case the experimental duration is fixed for two days (~120 shots). As shown in Fig. 3-6 (a), the total pressure in the case of 200 ˚C is lower than that of 30 ˚C until ~40 seconds after the start of heating CSP. Main component of desorbed gas is confirmed to be water at low temperature of the thermal desorption experiment (below ~400 ˚C). The partial pressure of m/e=18 (water molecule) is considerably reduced in the early period of the thermal desorption experiment (≤ 40 seconds, Fig. 3-6 (c)). It is considered that released gas comes from CSP, since the temperature of the wall surrounding CSP does not increase so much in the early period. Therefore this partial pressure difference between two experiments is mainly ascribed to the decrease of water molecules adsorbed on the CSP.

Figure 3-6 also shows that both the total and partial pressure in the case of 200 ˚C are higher than those of 30 ˚C after 40 seconds from the start of heating CSP. As to m/e=18, it is unlikely that further water molecules are desorbed from CSP, because the temperature of CSP is over 600 ˚C after ~40 seconds. Though the inner wall

temperature of vacuum vessel is not measured, it is supposed that the wall temperature in the 200 ˚C experiment is higher than that in the case of 30 ˚C. Thus the increase of total and partial pressure after ~40 seconds is probably caused by released gas from the wall of vacuum vessel.

Figure 3-7 shows the relation between the operational temperature of CSP and the time integration of partial pressure of m/e=18. The time integrated partial pressure of m/e=18 decreases with increase of the operational temperature of CSP below 200 °C. However, the values are hard to decrease above 200 ˚C. The above results indicate that a very high operational temperature is not required because the increased temperature of carbon material reduces the total amount of trapped particles.

3.4 Evaluation of the pumping efficiency

The time evolution of the total pressure during discharges in the case with CSP-off is explained by the following pressure-balance equations:

$$V_m \frac{dP_{CSP}^{off}}{dt} = C_m\left(P_{CC} - P_{CSP}^{off}\right) - S_m P_{CSP}^{off} + AS\Gamma_{CX} \ , \tag{3-8}$$

while in the case of CSP-on:

$$V_m \frac{dP_{CSP}^{on}}{dt} = C_m\left(P_{CC} - P_{CSP}^{on}\right) - S_m P_{CSP}^{on} + AS(1-\xi)\Gamma_{CX} \ , \tag{3-9}$$

where V_m is the volume of the test module, P_{CSP}^{on} and P_{CSP}^{off} the total pressure in the test module in the cases of CSP-on and -off, respectively. C_m is the conductance between the test module and GAMMA 10, S is the area of CSP, and A is the coefficient relating particles/sec to Pa·m^3/sec. S_m is the effective pumping speed of the turbo molecular pump installed on the test module and ξ is the pumping efficiency which is defined as the number of trapped particles divided by that of incident ones. It is assumed that the time evolution of P_{CC} is equal for cases of CSP-on and -off. The number of trapped

particles is obtained by using Eq. (3-8) and (3-9) as follows:

$$AS\xi\int_{t_0}^{t_d}\Gamma_{CX}dt = V_m\left(P_{CSP}^{off}-P_{CSP}^{on}\right)\Big|_{t=t_d} + \left(S_m+C_m\right)\int_{t_0}^{t_d}\left(P_{CSP}^{off}-P_{CSP}^{on}\right)dt, \qquad (3\text{-}10)$$

where t_0 is the starting time of plasma and t_d is the termination time of plasma. The number of trapped particles by CSP is estimated from the time evolution of the total pressure by use of Eq. (3-10). The number of incident particles Γ_{CX} is estimated from plasma parameters such as the diamagnetism, the line density measured with microwave interferometer, and the neutral atomic density was estimated by use of the results calculated by DEGAS [46, 47]. Radial density distribution and ion temperature profile are assumed to be Gaussian which have typical FWHM obtained from experimental data.

As shown in Fig. 3-8, the number of trapped particles increases with that of incident ones. Although the data are scattered to some extent, the pumping efficiencies ξ of CSP are estimated to be 0.65 and 0.66 for the cases of 30 ˚C and 200 ˚C, respectively. Data of incident fast neutrals are almost in the range of $1\sim4\times10^{14}$ (H), because many experiments are carried out under the similar parameters. The above results also indicate that the reduction of pumping efficiencies are small in the application to actual devices. There is no remarkable difference between two operational temperatures within the experimental error.

3.5 Thermal desorption experiment

In the regeneration phase, CSP is heated up to ~800 ˚C by the resistive heating. This annealing process is not only for regeneration of CSP but also for investigating the behavior of hydrogen reemission [38, 39]. In the thermal desorption experiments, the terms concerning ion irradiation are negligible. Thus the mass-balance equations are modified into the following forms [48]:

$$\frac{dn_M(t)}{dt} = \Sigma_d n_T(t) - \Sigma_T n_M(t)\left[C_0 - n_T(t)\right] - 2K_1 n_M(t)^2, \tag{3-11}$$

$$\frac{dn_T(t)}{dt} = -\Sigma_d n_T(t) + \Sigma_T n_M(t)\left[C_0 - n_T(t)\right]. \tag{3-12}$$

When it is assumed that $n_M(t)$ reaches a quasi steady state simultaneously after start of the annealing because of strong retrapping effect, the decay profile due to the hydrogen molecule emission is expressed as follows:

$$\frac{C_0}{n_T(0)}\left[1 - \frac{1}{N_T(t)}\right] - 2\ln\left[N_T(t)\right] + \frac{n_T(0)}{C_0}\left[N_T(t) - 1\right] = -\frac{2K_1}{C_0}\left[\frac{\Sigma_d}{\Sigma_T}\right]^2 t, \tag{3-13}$$

where $N_T(t)$ is $n_T(t) / n_T(0)$. The numerical coefficient of the right hand side of Eq. (3-13) is defined as the effective recombination rate constant K_{eff}. The desorption spectrum is proportional to the first derivative of $n_T(t)$ in the case of high pumping speed [38]. Hence K_{eff} is given by setting the second derivative of $n_T(t)$ zero [49]:

$$K_{eff} = K_0 \exp\left(\frac{E_\tau}{k\left(T_m + T_0\right)}\right) = \frac{\left(1 - \frac{n_T(0)}{C_0}\right)}{\frac{n_T(0)}{C_0}} \frac{1}{t_m} \frac{E_\tau}{E_\tau + 0.2}, \tag{3-14}$$

where K_0 denotes the pre-exponential factor, E_τ is the activation energy and t_m is the time of the peak pressure. T_0 and T_m are the initial and the peak temperature.

Figure 3-9 (a) shows the thermal desorption spectra of hydrogen pressure. The duration of the experiments are 1, 2, and 3 days and the operational temperature of CSP is kept at 200 ˚C. The adsorbed gas on the CSP surface is not negligible since the pressure rise is observed even in the case of the 200 ˚C experiment. The background gas is assumed to be a liner function. The corrected desorption spectra are shown in Fig. 3-9 (b) and t_m is estimated from this figure. The initial density is estimated from the fluence of fast neutrals and the depth profile of hydrogen measured with ERD and calculated by the TRIM code (see chapter 4).

The Arrhenius plot of the effective recombination rate constant is shown in Fig. 3-

10. The activation energy and the pre-exponential factor are estimated to be 1.80 eV and 6.24 x 10^{12} s^{-1}. The value of K_{eff} is corresponding to the low density experiment [50].

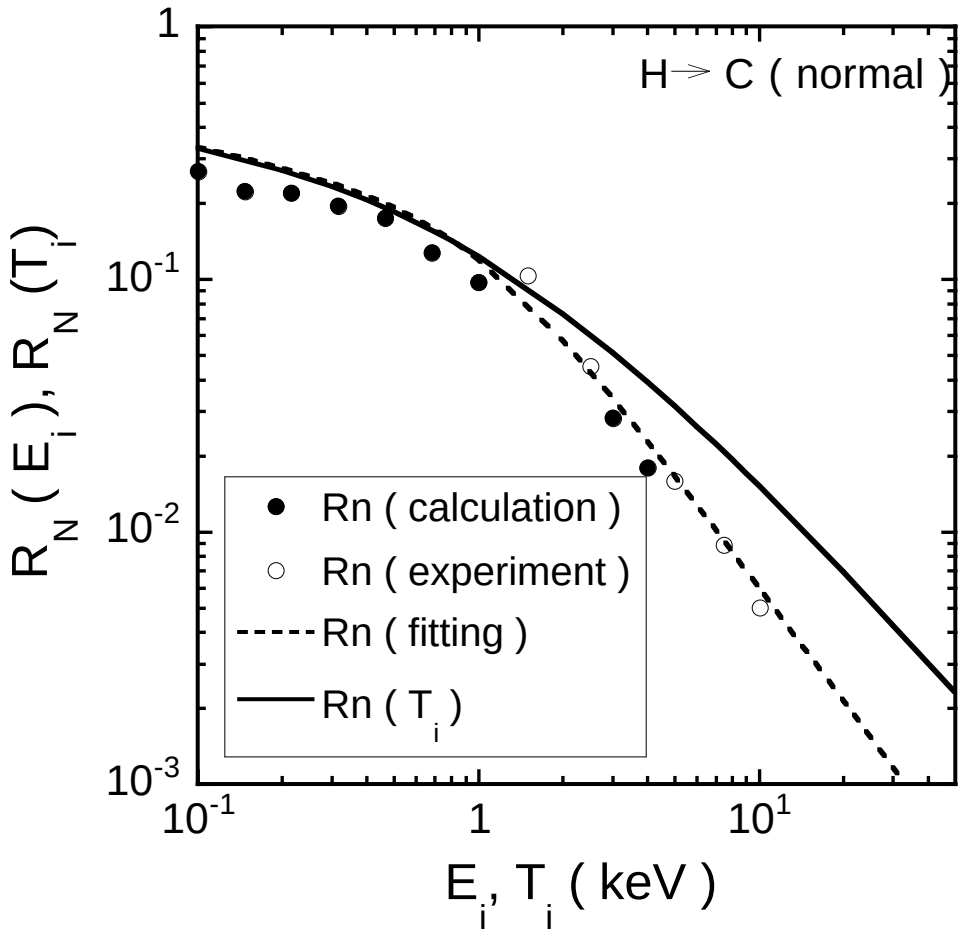

Fig. 3-1 Reflection coefficient of carbon material. Rn (fitting) is calculated from Eq. (3-1) and (3-2). $R_n(T_i)$ is also evaluated from Eq. (3-3).

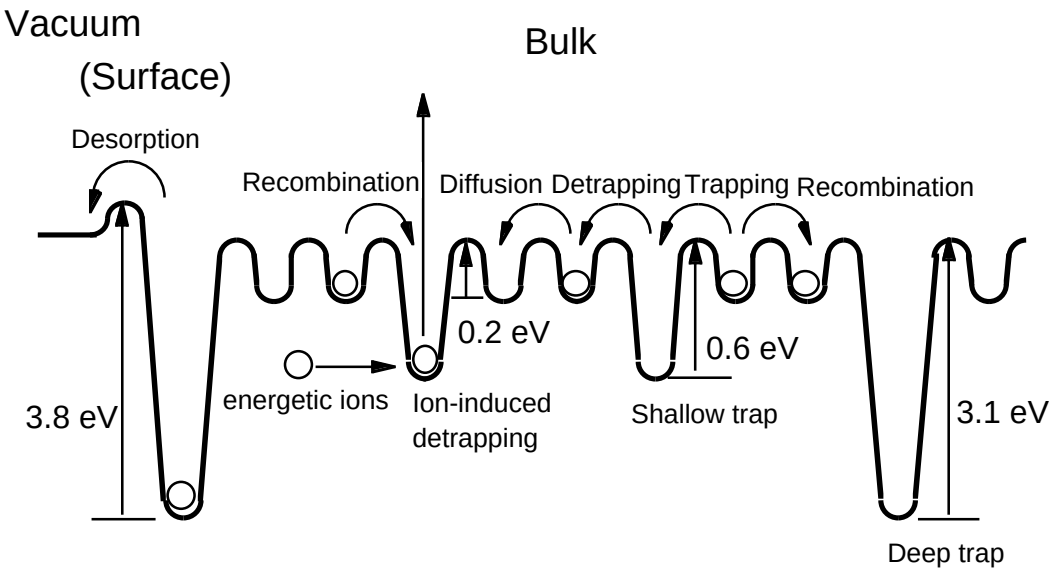

Fig. 3-2 Schematic diagram of the hydrogen transport in the carbon material proposed by Morita

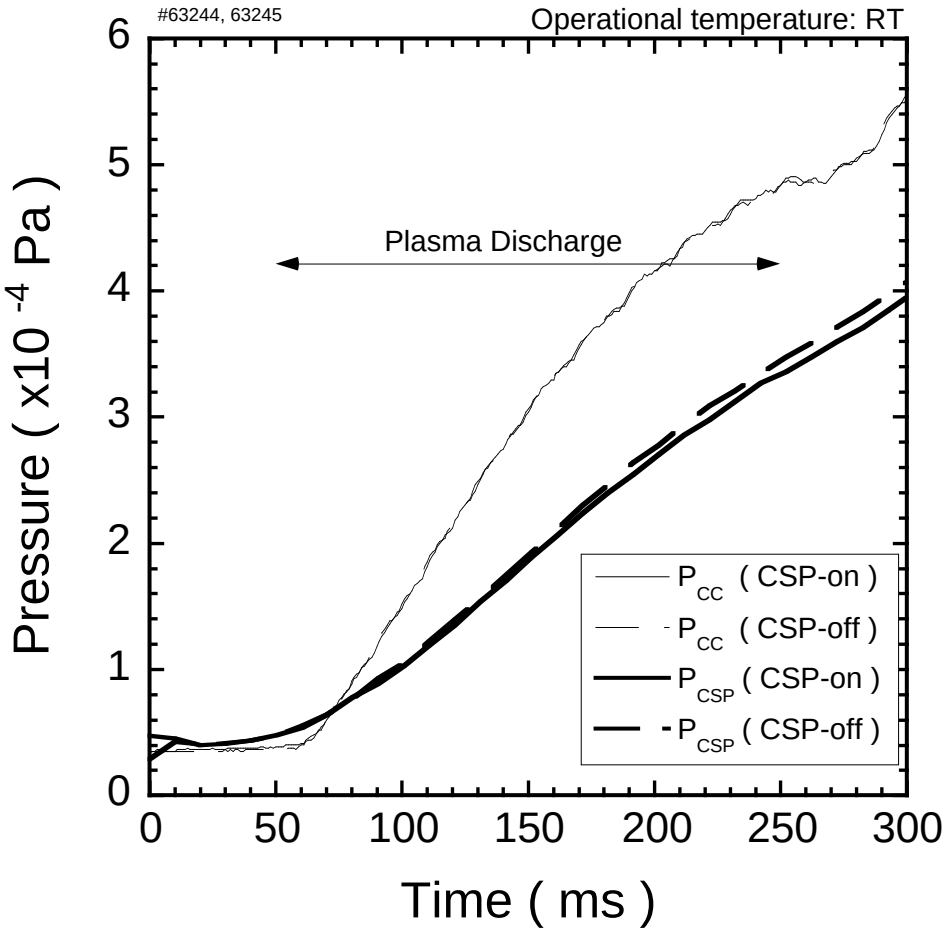

Fig. 3-3 Time evolution of hydrogen pressures in the test module and the central cell in the cases of CSP-on and -off at RT.

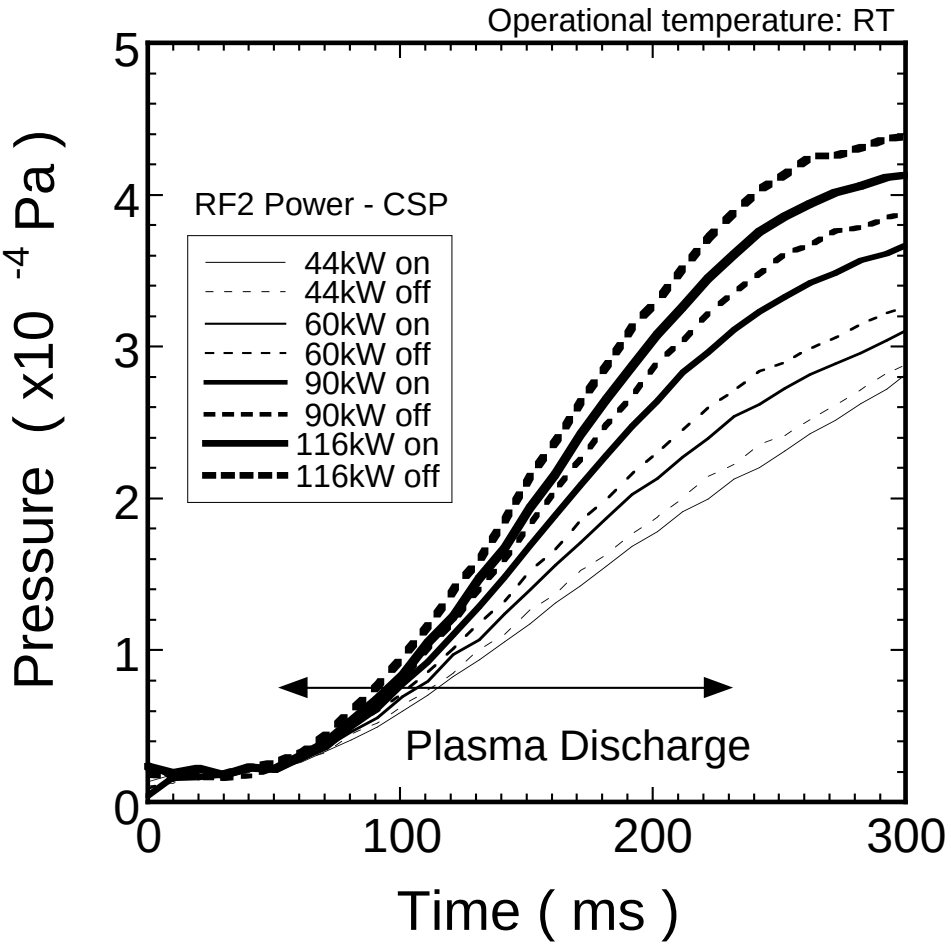

Fig. 3-4 Heating power dependence of pressure difference in the CSP test module.

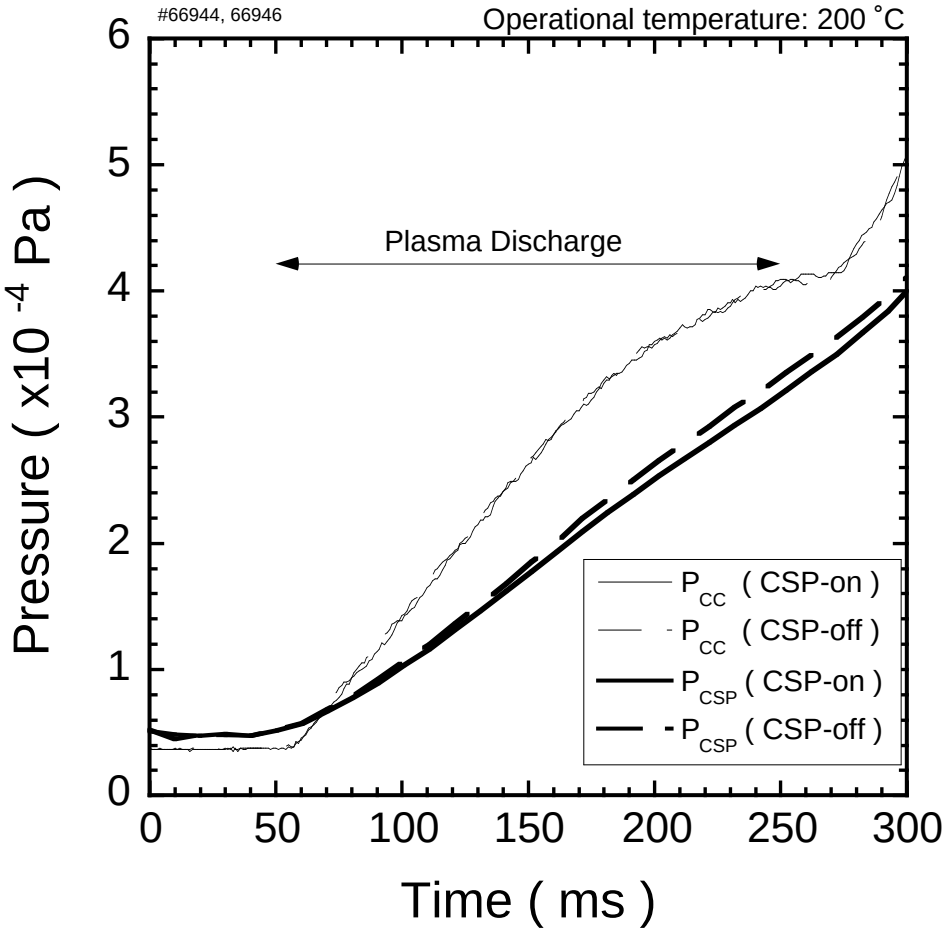

Fig. 3-5 Time evolution of hydrogen pressures in the test module and central cell in the cases of CSP-on and off at the temperature of 200 ˚C.

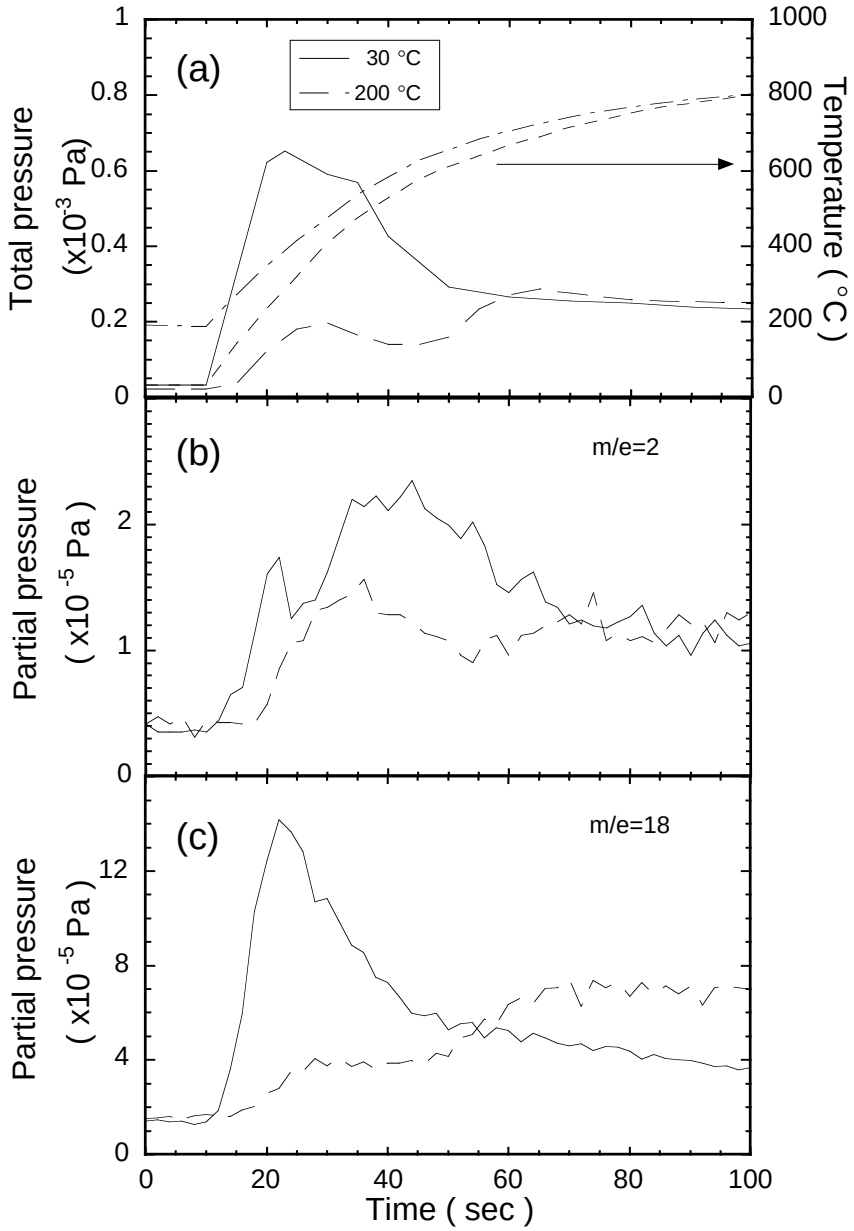

Fig. 3-6 Temporal evolution of (a) total and partial pressures ((b) hydrogen and (c) water molecule) in the thermal desorption experiment at the temperature of RT and 200 ˚C.

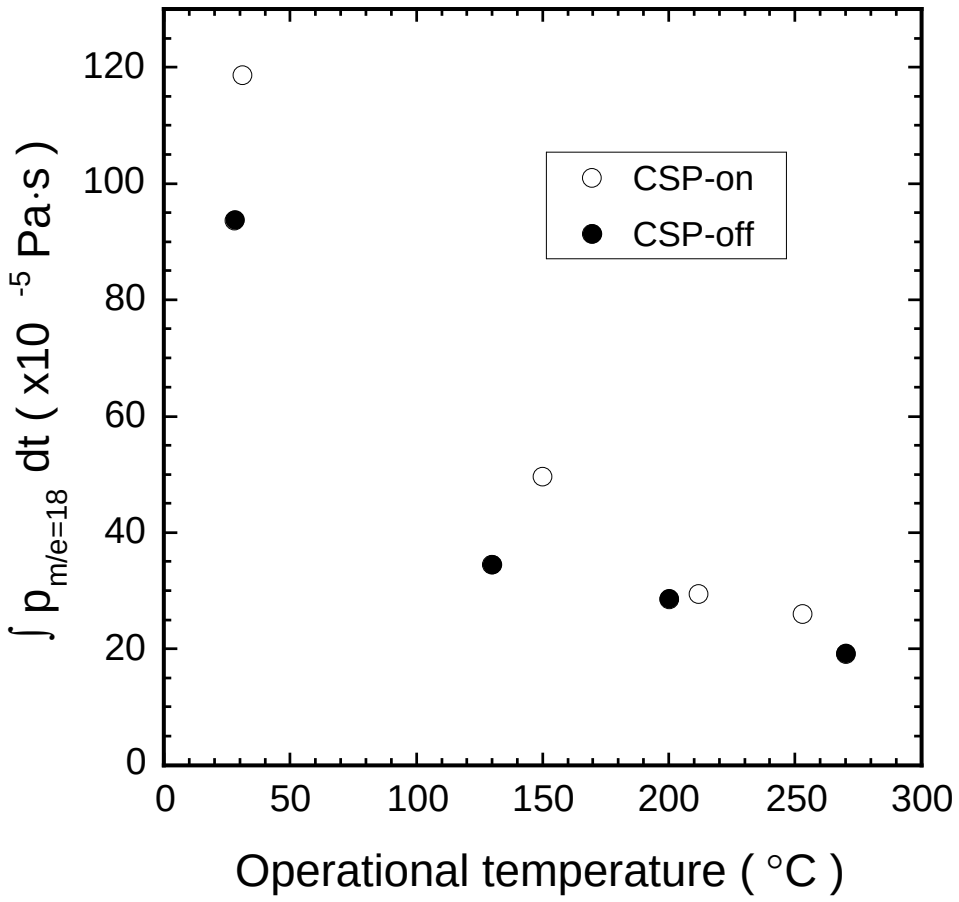

Fig. 3-7 Temperature dependence of the quantity of adsorbed water molecule in the cases of CSP-on and off.

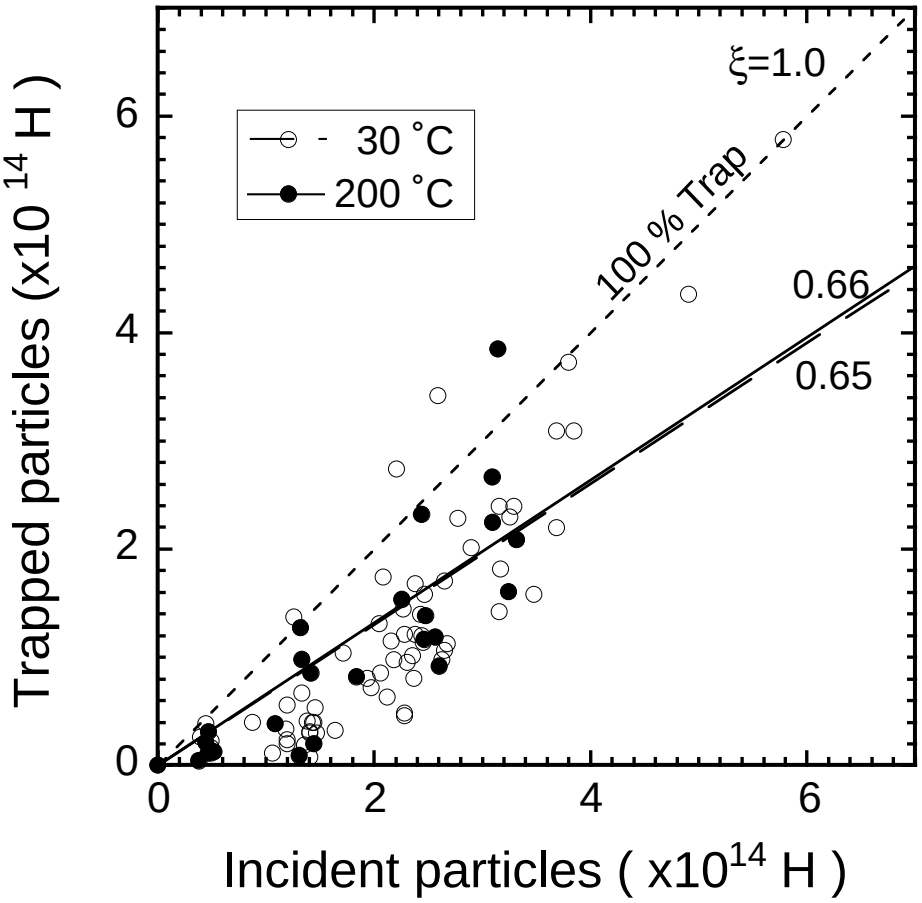

Fig. 3-8 Correlation between the number of incident particles and that of trapped ones during plasma discharges.

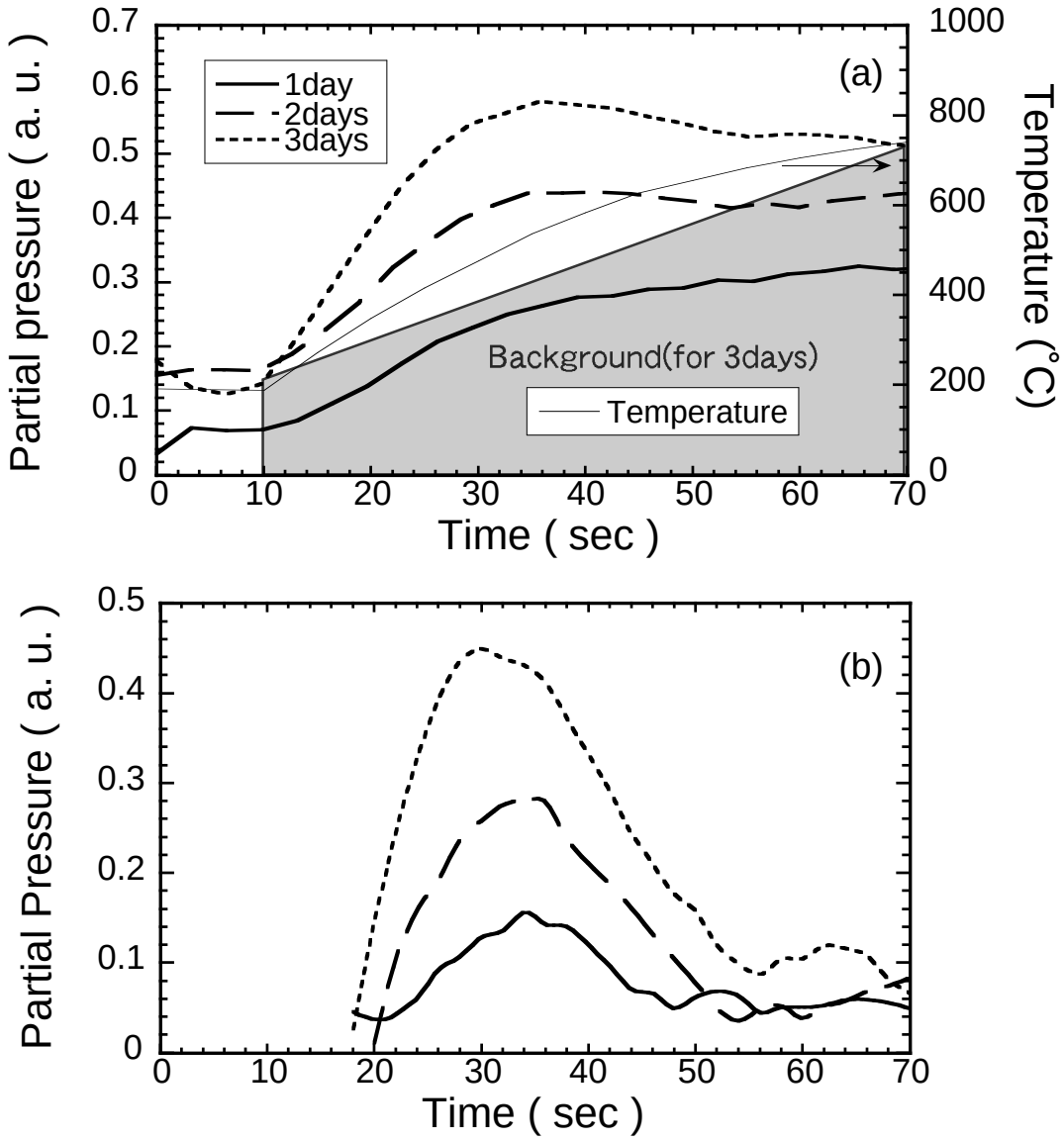

Fig. 3-9 Thermal desorption spectra of hydrogen molecule. (a) raw data, (b) corrected data. The operational temperature of CSP is 200 °C.

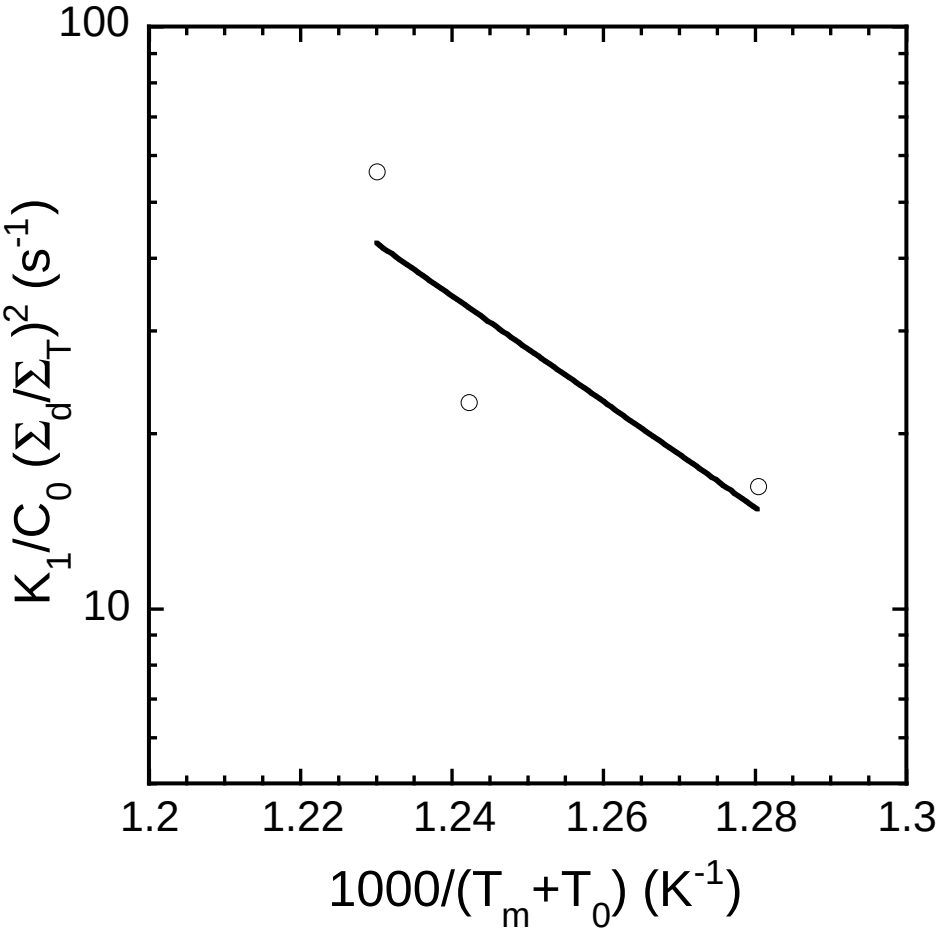

Fig. 3-10 The Arrhenius plot of the effective recombination rate constant.

4. Surface analysis of CFC materials

4.1 Methods of surface analysis

4.1.1 Elastic recoil detection

Light elements in the substrate can be detected by the elastic recoil detection analysis (ERD) [51]. The schematic configuration of ERD is shown in Fig. 4-1 (a). As shown in the figure, the particle recoiled by the incident probe is injected into the detector and is analyzed its energy to generate the energy spectrum. The yield of recoiled atom per 1 channel of multi-channel analyzer (MCA), Y is given by,

$$Y = N \cdot Q \frac{d\sigma}{d\Omega} \Delta\Omega \frac{1}{\sin\alpha} \frac{E_c}{\frac{dE}{dx}}, \tag{4-1}$$

where N is the density of target atom at the depth d, Q is the number of probe particle, $d\sigma/d\Omega$ is the recoil cross section, $\Delta\Omega$ is the solid angle of the detector, α is the incident angle respect to the substrate surface and E_c denotes the energy width of MCA. dE/dx is the stopping power at the depth and the energy [54-57].

In ERD, the depth profile can be obtained by analyzing the energy of the target atom collided with the probe particle because the energy of the target and probe particle are decreased by the stopping power determined by their charge, energy and mass. The energy decrement of the probe and recoiled particles is expressed as follows:

$$E_1 = E_0 - \int_0^{\frac{d}{\sin\alpha}} \frac{dE}{dx}_{in} dx, \tag{4-2}$$

$$E_2 = k_r E_1, \tag{4-3}$$

$$E_3 = E_2 - \int_0^{\frac{d}{\sin\beta}} \frac{dE}{dx}_{out} dx, \tag{4-4}$$

$$E_4 = E_3 - \int_0^{t} \frac{dE}{dx}_{filter} dx, \tag{4-5}$$

$$k_r = \frac{4M_1M_2\cos^2\phi}{M_1 + M_2}, \tag{4-6}$$

where E_0 is the incident energy of the probe particle, E_1 is the energy just before collision with the target atom, E_2 is the transferred energy from the probe particle, E_3 is the energy of the recoiled atom right after ejection from the substrate and E_4 is the detected energy at SSD. dE/dx_{in}, dE/dx_{out} and dE/dx_{filter} are the stopping powers along the inward, outward paths and in the filter. k_r denotes the recoil kinetic factor. ϕ is the recoil angle. Not only recoil of the target atom but also forward scattering of the probe particle occur in this configuration. Utilizing the difference of stopping power between the recoiled and the scattered particle, the material and the thickness of the filter is determined so that the scattered particle is completely stopped at the filter and that the most of recoiled particles can penetrate the filter. Mylar and aluminum on the order of micro mater are usually used as the filter. An aluminum filter of 7 μm is used in the present apparatus.

4.1.2 Rutherford backscattering spectroscopy (RBS)

As shown in Fig. 4-1 (b), particles of incident beam collide with target atoms and are scattered backward into the detector. The energy ratio of incident to scattered particle, called the kinetic factor, is determined by only the scattering angle and mass of probe and target particle. When the scattering angle θ is given, the kinetic factor k is expressed as follows:

$$k = \left\{ \frac{M_1\cos\theta + \sqrt{M_2^2 - M_1^2\sin^2\theta}}{M_1 + M_2} \right\}^2, \tag{4-7}$$

the energy decrement along inward and outward paths are expressed as similar as that of ERD,

$$E_1 = E_0 - \int_0^{\frac{d}{\sin\alpha}} \frac{dE}{dx}_{in} dx, \tag{4-8}$$

$$E_2 = k\, E_1, \tag{4-9}$$

$$E_3 = E_2 - \int_0^{\frac{d}{\sin\beta}} \frac{dE}{dx}_{out} dx, \tag{4-10}$$

where E_2 is the energy after the collision with the target atom, E_3 is the energy of the probe particle right after ejection from the substrate. Thus the depth profile of the quantity of each element in the substrate can be obtained by the energy spectrum of RBS.

4.2 Experimental Results

The hydrogen depth profile of exposed C/C material is different from that of annealed one as shown in Fig. 4-2. The experimental data are noticeably scattered owing to large surface roughness of the C/C material and low fluence of fast neutrals. From the count number of recoiled atoms, the hydrogen density in the material can be evaluated in this analysis. This difference is considered to be caused by fast neutrals trapped by C/C material. The pumping effect of CSP has been estimated by the pressure difference between with and without CSP during plasma discharges. It has been confirmed for the first time from the microscopic viewpoint that fast neutrals emitted from plasmas generated by the actual confinement device (GAMMA10) are trapped by the C/C material.

Figure 4-3 (a) shows the RBS energy spectra of exposed and annealed C/C materials. The channel number depends on the backscattered helium energy and the depth of a target atom. Both spectra roughly overlap each other. As shown in Fig. 4-3 (b) (magnified figure of high-energy side), a minute amount of oxygen (< 1 %) has been detected on the surface of the exposed sample. However, no serious problem probably

occurs for the pumping performance of CSP because the analysis was conducted after ventilation and the quantity of oxygen was significantly smaller compared with that of carbon.

4.3 Analysis of experimental data by the TRIM code

4.3.1 The Monte Carlo simulation code TRIM

The TRIM code can calculate the transport and ranges of incident ions in materials on the assumption that the collision between ions and material atoms can be treated as the binary collision approximation (BCA). The BCA model does not hold at low energy when many-body effects become important. The energy range treated in this thesis satisfies this requirement. Since the details of the simulation of ion-solid interactions are written in Ref. [58], the outline of the code is described here. The origin of the TRIM code [59], which can calculate only range of ions, was developed in 1980 by Beirsack and Haggmark. Some versions of the code, which can treat tracking of recoils, sputtering and diffusion of ions in the material, are available with a variety of improvements by Eckstein et al. In this thesis, TRIM.SP [60] (ver. TRVMC95) is used.

It is assumed that the collision between incident and target atom with impact parameter p determined randomly occurs after the flight of mean free path λ. The above routine repeats until the energy reaches below the cut off energy (stop and capture in the material) or ejection from the surface (reflection).

4.3.2 Hydrogen depth profile calculated by the TRIM code

Numerical simulations are carried out by means of the Monte Carlo simulation code TRIM for comparison to the ERD results [22]. Ions are used as the substitute of fast neutrals in the numerical calculation. It was found that the energy spectrum of the

charge exchange fast neutral emitted from GAMMA 10 plasma is expressed as a superimposing of Maxwell-distributed low temperature bulk component (~90 %) on Maxwell-distributed high energy tail (~10 %) [33]. The calculations are performed taking into account these two components. The experimental result qualitatively agrees with numerical calculation at the bulk ion temperature of 2 keV and the tail temperature of 20 keV as shown in Fig. 4-4. Circles show the count of the hydrogen atom obtained by subtracting the count of the annealed sample from that of the exposed sample in order to estimate the hydrogen density due to fast neutrals. The ion temperature of 2 keV also agrees with a typical bulk ion temperature of GAMMA10 plasmas (0.5 ~ 5 keV). It seems that projectiles are trapped by carbon near each projected range. This result contributes to estimate the regeneration cycle of CSP.

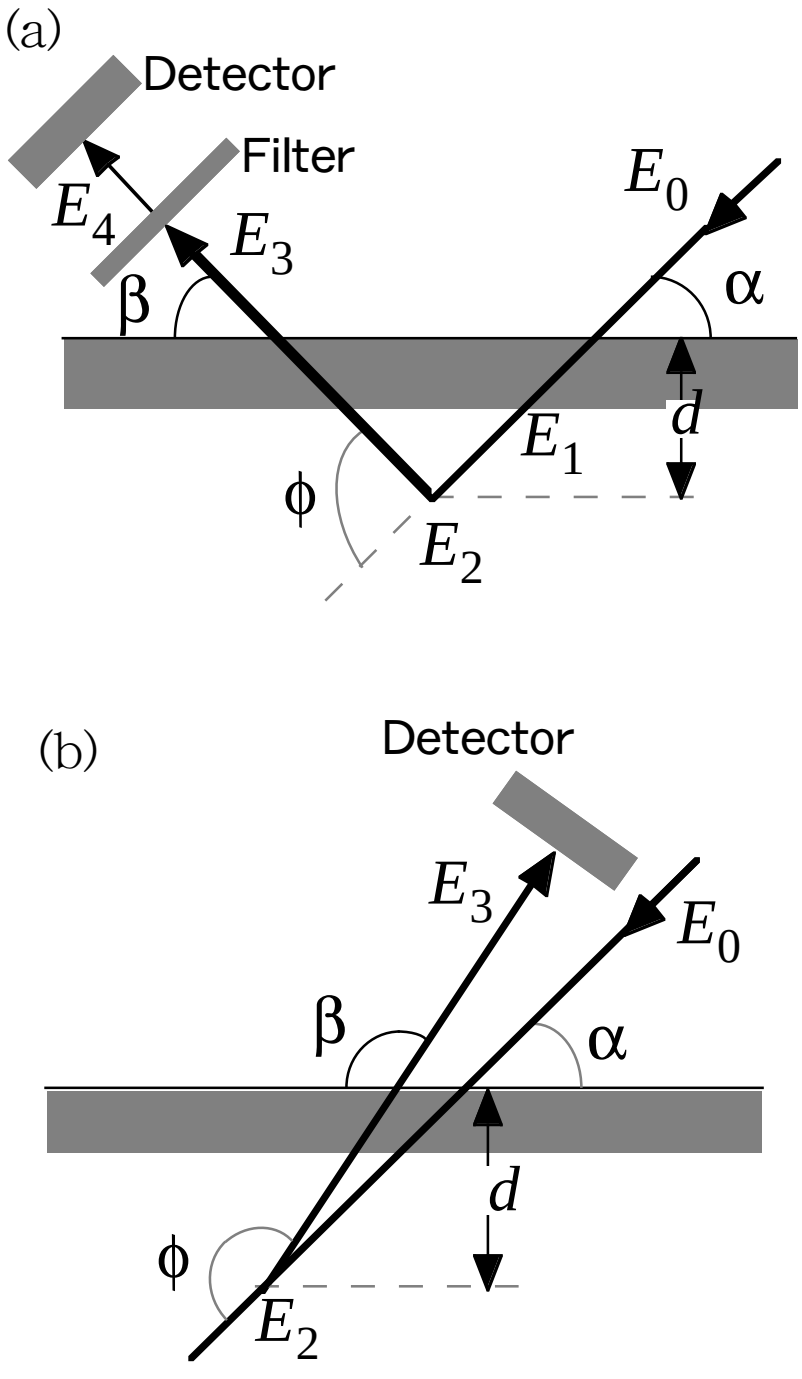

Fig. 4-1 Schematics of (a) Elastic Recoil Detection (ERD) and (b) Rutherford Backscattering Spectroscopy (RBS) analyses.

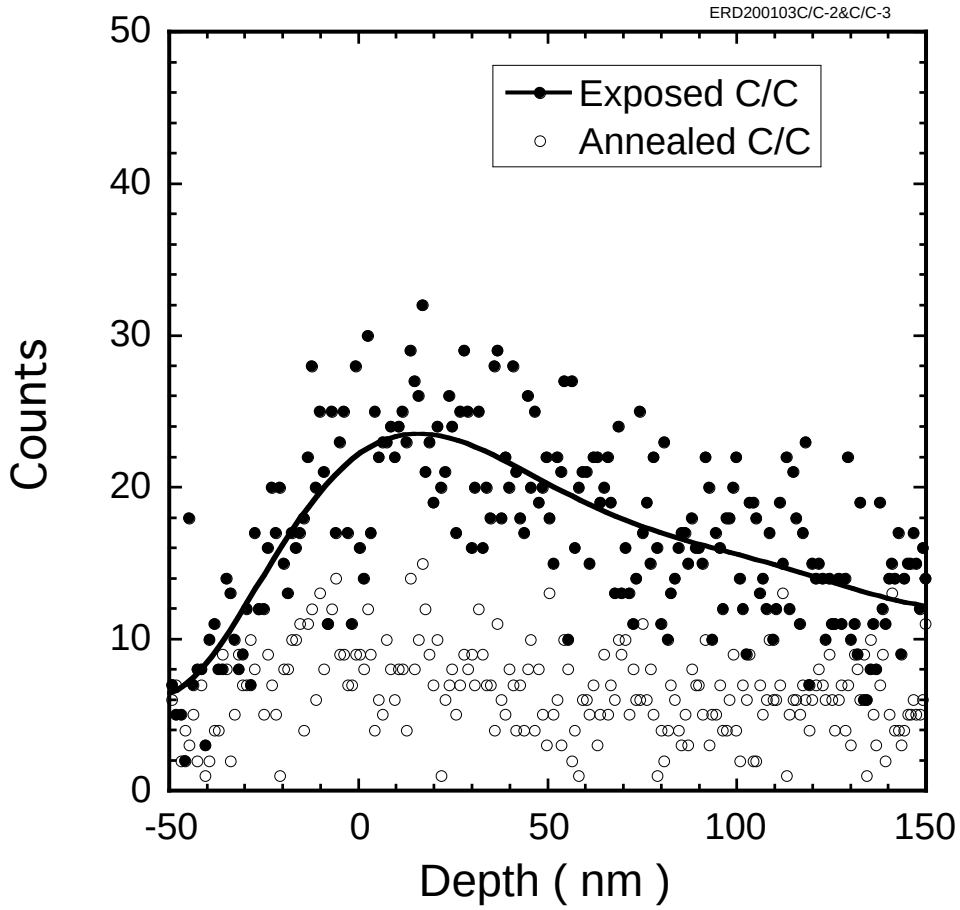

Fig. 4-2 Depth profiles of Hydrogen density in the samples. Solid line is drawn to guide the eye.

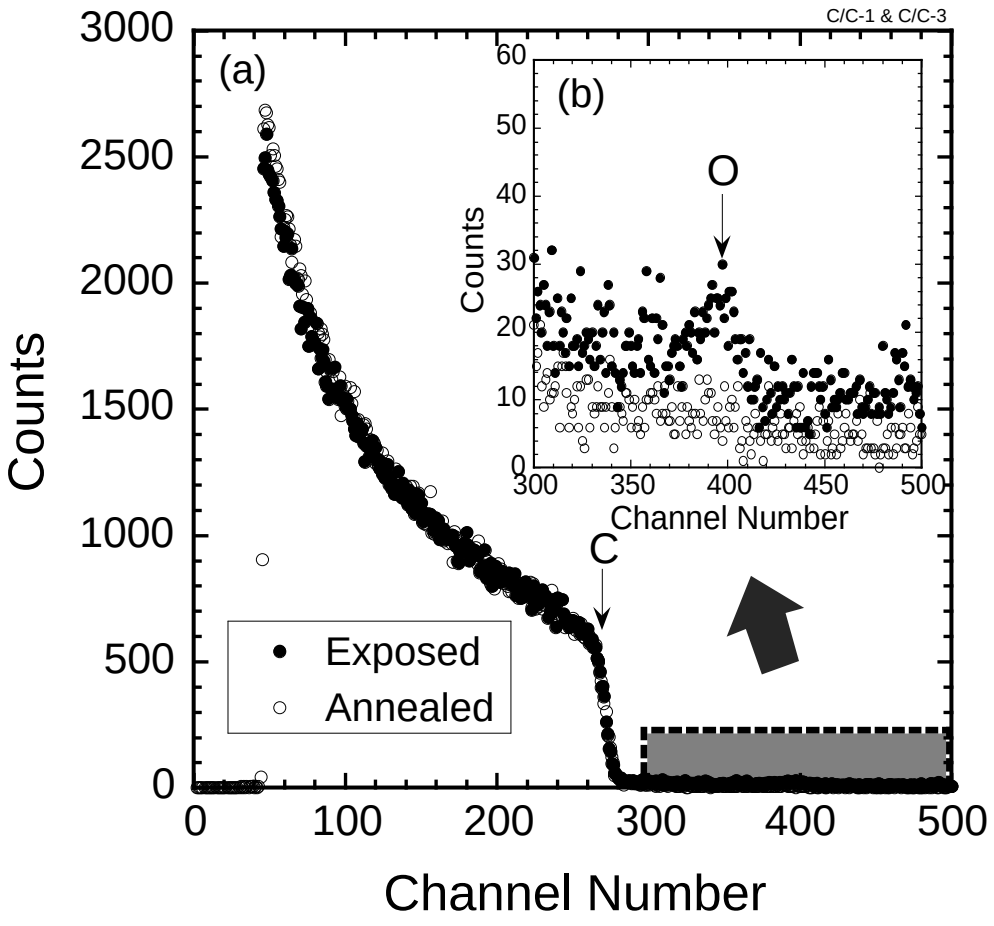

Fig. 4-3 RBS spectra of the samples. (a) Whole spectra, (b) a magnification of high-energy side.

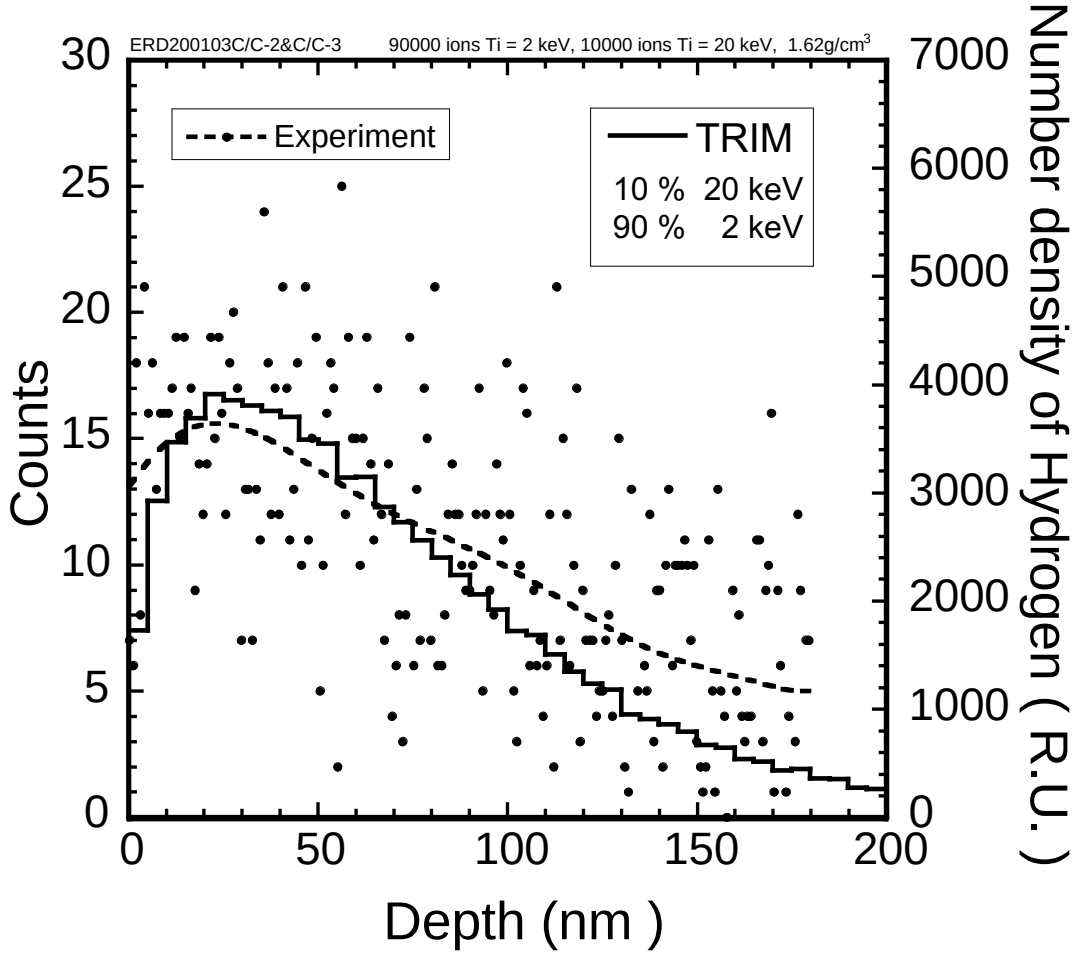

Fig. 4-4 Comparison hydrogen density due to fast neutrals and the calculation result by using the TRIM code

5. Application of CSP under the condition of high heat and particle load

5.1 The motivation of the CSP beam dump

So far, it has been considered that CSP is applied under low heat flux circumstance since a high temperature leads to decrease of a total amount of hydrogen retention in carbon materials and also enhances the chemical sputtering [26]. Moreover it is reported that phenomena called carbon bloom [61] is caused by the influence of radiation enhanced sublimation which occurs on the surface of the damaged carbon material above ~1000 ˚C. However, heat and particle load to the first wall has a tendency to increase with improvement of plasma performance and extended pulse length. Therefore in order to study the capability of CSP under high heat flux circumstance, CSP is newly applied to the shine-through beam dump of NBI.

There is another reason to apply CSP to GAMMA 10. The schematic illustration of neutral particle flow (both hot and cold) is shown in Fig. 5-1. In the present plasma parameters of GAMMA 10 (nl ~ 5 x 10^{17} m^{-2} and T_e ~ 60eV), about 95 % of incident beam passes through the plasma column and becomes a large amount of hydrogen molecule in the dump tank. The back-flow due to this shine-through beam must be reduced in order to suppress the charge exchange loss. Hence CSP is applied to the beam dump for NBI.

5.2 The thermal design of the CSP beam dump

The temperature rise of carbon material due to heat influx has an influence on the pumping capability of CSP. Before designing CSP for shine-through beam dump

(CSPBD), the heat transport in CSP is calculated in the cases of the carbon material used in the test module (CX-270) and of high heat conductive C/C material (CX-270G). The physical properties of these materials are tabulated in Table 5-1. A 2-dimesional heat transfer equation is solved as a finite difference equation. The schematic drawing of calculation is shown in the Fig. 5-2. The gaussian-distributed heat flux is given on the surface. The e-holding length of the beam intensity at CSPBD is about 0.16 m.

The results are shown in Figs. 5-3 and 5-4. The initial temperature and the heat flux at the beam center are set to be 20 ˚C and 4 MW/m^2, respectively. Maximum pulse length of NBI is 100 ms in the present GAMMA 10 experiment. The temperature of the beam center exceeds 300˚C after 30 ms irradiation in the case of CX-270. There is the possibility of the degradation of pumping capability and increase of sputtering yield. In the case of CX-270G, incident angle is 60˚ with respect to the normal surface in order to reduce the heat flux. The surface temperature is kept less than 200 ˚C even after the 100

		Unit	CX-270 (CSP test module)	CX-270G (CSPBD)
Temperature of heat treatment		˚C	~ 2000	~ 3000
Density		kg/m^3	1660	1690
Bending strength	⊥	MPa	180	140
Tensile strength	//	MPa	230	170
Resistivity	//	μΩ m	18	9
Thermal expansion coefficient	//	10^{-6}/K	<1	<1
(RT~1273 K)	⊥		7.7	9.5
Themal conductivity	//	W/m K	35	155
(RT)	⊥		5	24

Table 5-1 The physical properties of CX-270 and CX-270G.

ms irradiation. The earlier result described in chapter 3 shows that the pumping efficiency has no remarkable difference between the cases of CSP temperature of 30 ˚C and 200 ˚C. Accordingly, this result suggests that CSP is suitable for this purpose under the present experimental condition by the use of high heat conductive materials.

5.3 Pumping Experiment

Figure 5-5 shows the results of pumping experiment in the cases of CSP-on and -off. The energy and current of NB is approximately 21 keV and 20 A, respectively. The beam pulses are 10, 20 and 30 ms, respectively. The measured pressures in the case of CSP-on are lower than that of CSP-off in the same pulse length. The pressure difference increases with the NB pulse length. This result indicates the pumping effect of CSP on NB. However, due to a larger amount of gas flow from the ion source than the back-flow from the dump tank, the pressure difference between CSP-on and off has not been observed in the central cell.

In order to quantitatively evaluate these results, a pressure-balance analysis is performed under the assumption that the system consists of the central region and the dump tank as shown in Fig. 5-6. The time evolution of pressure in the dump tank is expressed as follows:

$$V_{dump}\frac{dP_{dump}}{dt} = C_{dump}\left(P_{CC} - P_{dump}\right) - S_{dump}P_{dump} + \left(1-\xi\right)\Gamma_{NB} + Q_{wall}, \qquad (5\text{-}1)$$

where P_{CC} and P_{dump} are the pressures in the central cell and the dump tank, respectively. V_{dump} is the volume of the dump tank and S_{dump} is the effective pumping speed of the pumping system in the dump tank. Γ_{NB} is the flux of NB injected into the dump tank, ξ is the pumping efficiency of CSP defined as the ratio of number of trapped particles to that of incident ones and Q_{wall} is the gas flow from the wall of the dump tank. The gas flow from the inner wall of the dump tank is estimated by substituting the initial

pressures into the Eq. (5-1). Γ_{NB} and *dP/dt* are zero before the plasma discharge is initiated. It is assumed that Q_{wall} does not change during the plasma discharge. C_{dump} is the conductance between the central cell and the dump tank. Here, trapped particles by CSP involve ones desorbed by NB. The relation of the pumping efficiency and recycling coefficient of CSP γ_{CSP} is expressed as follows:

$$\gamma_{CSP} = 1 - \xi. \tag{5-2}$$

The correlation between the number of incident particles and that of trapped ones by CSP is shown in Fig. 5-7. The number of incident particles is estimated from the drain current of the ion source, the neutralization efficiency measured with arrays of Faraday-cups and calorimeter and from beam transport calculation. It is confirmed that the pumping efficiency is improved to be 0.60 to 0.82 by increasing the regeneration temperature from 600 ˚C to 750 ˚C. This value, 0.82, is equivalent to 150 m^3/s as an effective pumping speed. Figure 5-8 shows the fluence dependence of the pumping efficiency. As shown in Fig. 5-8, the pumping efficiency starts with a significantly low level and is drastically improved at the beginning of the irradiation. It is considered that the amount of particles adsorbed in an interval of plasma shots and that of desorbed particles by NB reach equilibrium immediately. Although the pumping efficiency decreases with increase of the number of incident particles, it has been experimentally confirmed that the pumping efficiency recovers to 0.80 from 0.69 by the regeneration as shown in Fig. 5-8. The beam center of CSP is considered to be saturated by the incident neutral beam when this regeneration experiment was conducted. The fluence of the center is estimated to be approximately five times larger than saturation (~10^{22} H/m^2). This result indicates that CSP can be used repetitiously.

The pumping efficiency of about 0.35 is obtained even in the case of CSP-off (beam is incident on the stainless shutter). The shutter is in front of CSPBD so as to protect the dump tank against the radiation from CSPBD in the regeneration experiment.

The temperature of the shutter is heated up to around 500 ˚C during the experiment. The pumping efficiency of the shutter may be explained from the low-outgassing rate due to baking and the particle reflection coefficient for high energy particles.

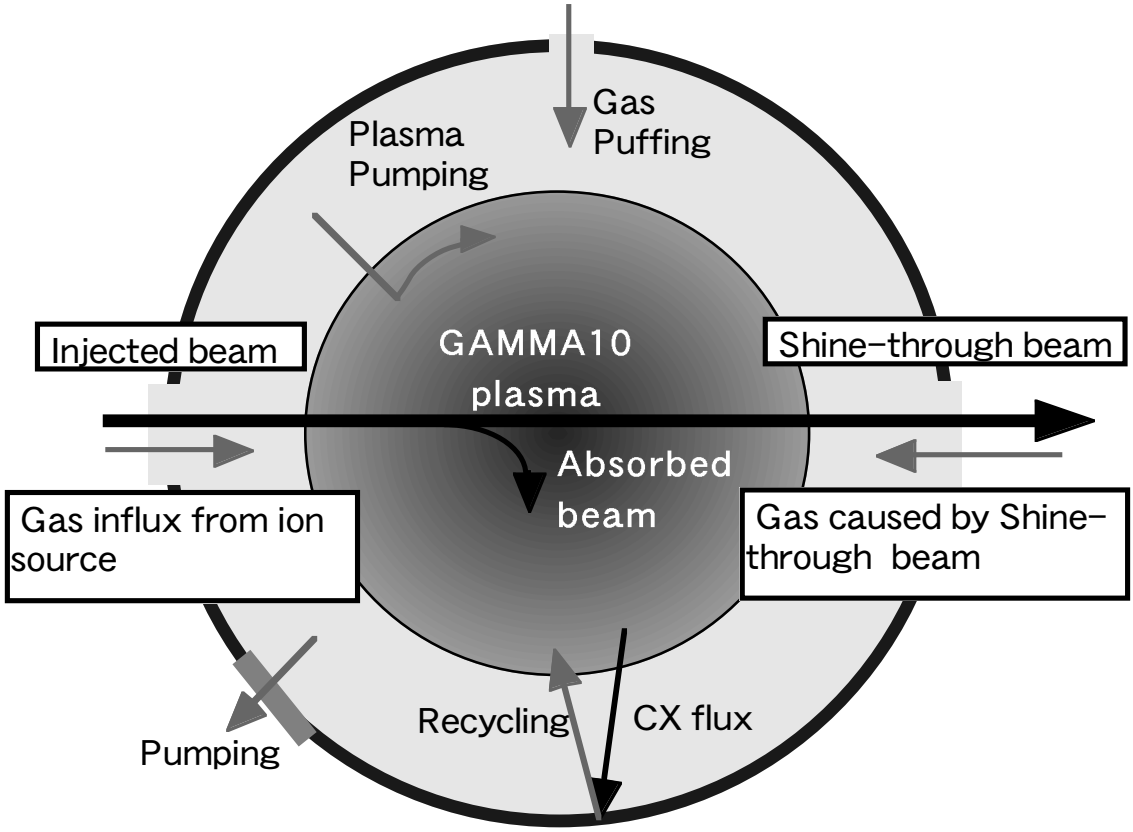

Fig. 5-1 A schematic of neutral particle flow in the central cell.

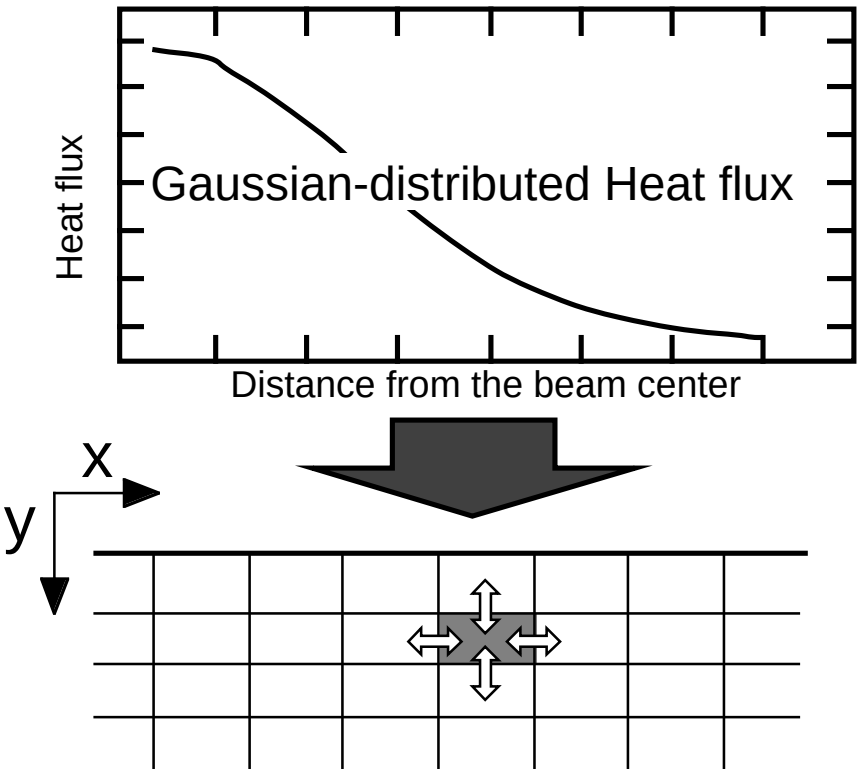

Fig. 5-2 A model of heat transfer calculation.

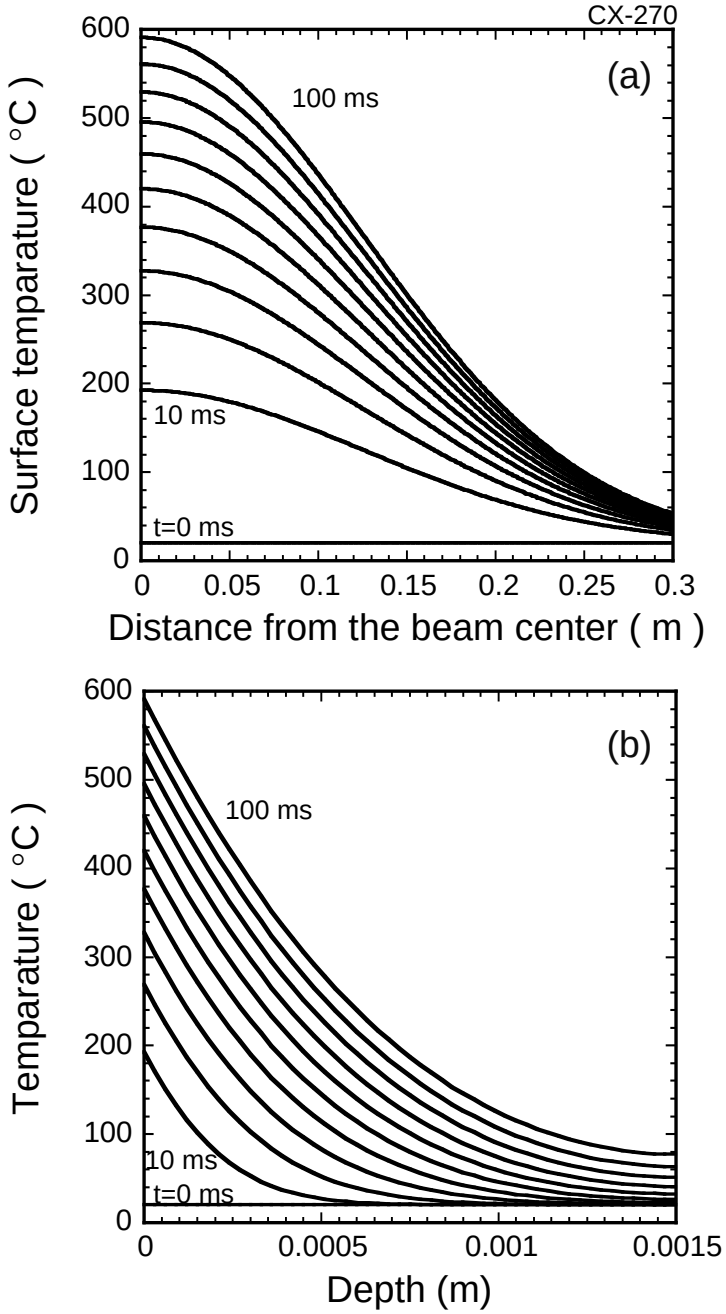

Fig. 5-3 The result of heat transfer calculation in the case of the C/C material (CX-270) used in the test module. The incident angle is assumed to be normal to the surface. Temporal evolution of (a) surface temperature and (b) depth profile of temperature at the beam center.

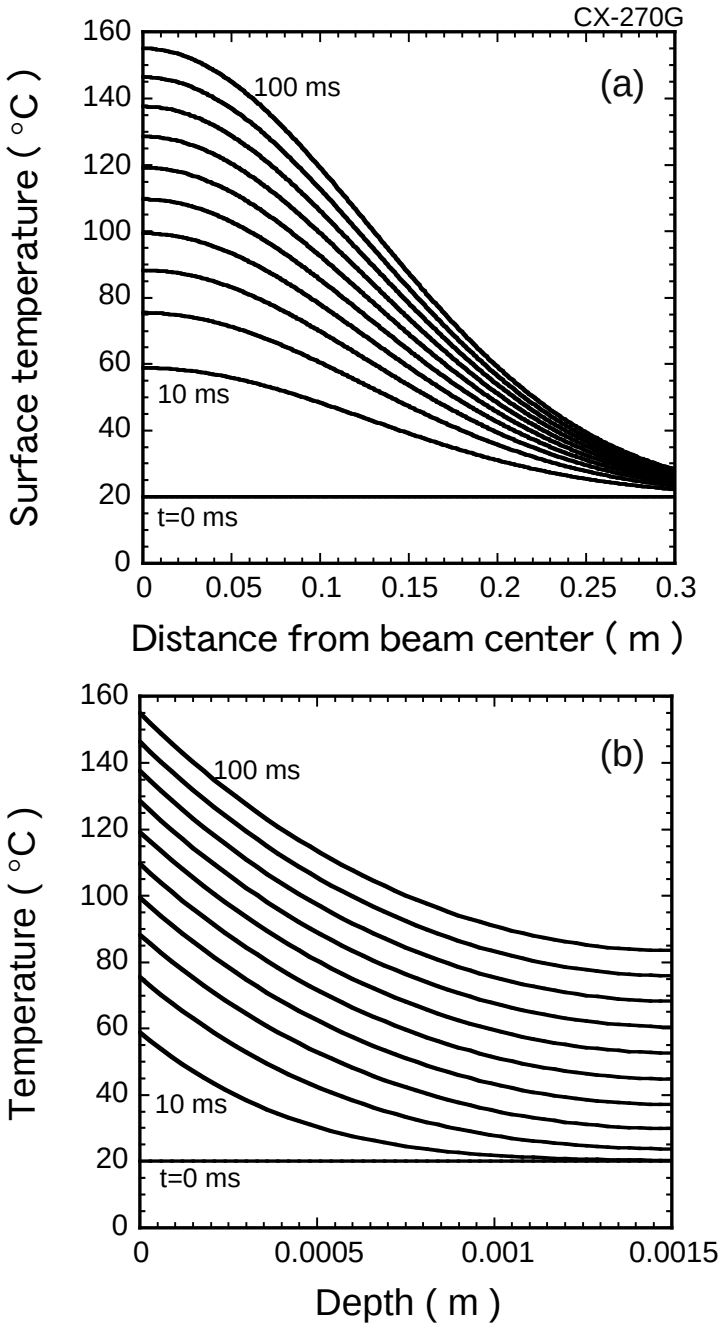

Fig. 5-4 The result of heat transfer calculation is the case of the high heat conductive C/C material (CX-270G). the incident angle is 60° to the surface normal in order to reduce the heat flux. Temporal evolution of (a) surface temperature and (b) depth profile of temperature at the beam center.

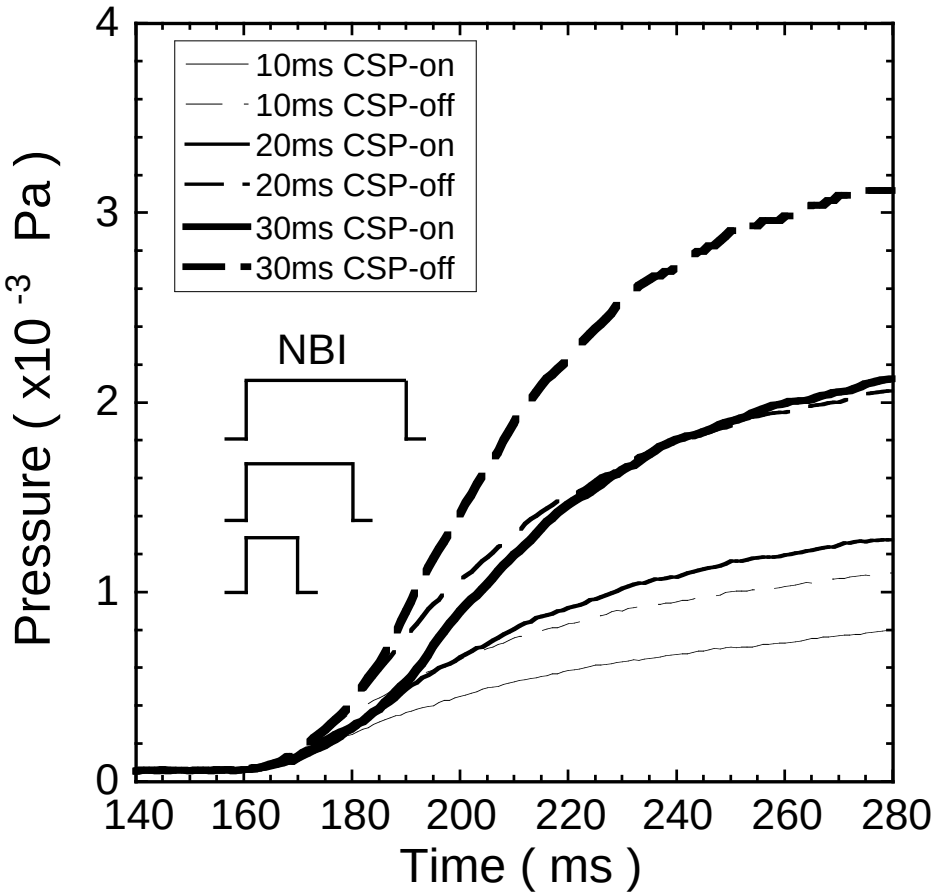

Fig. 5-5 Time evolution of neutral pressure in the dump tank during and after NB injection.

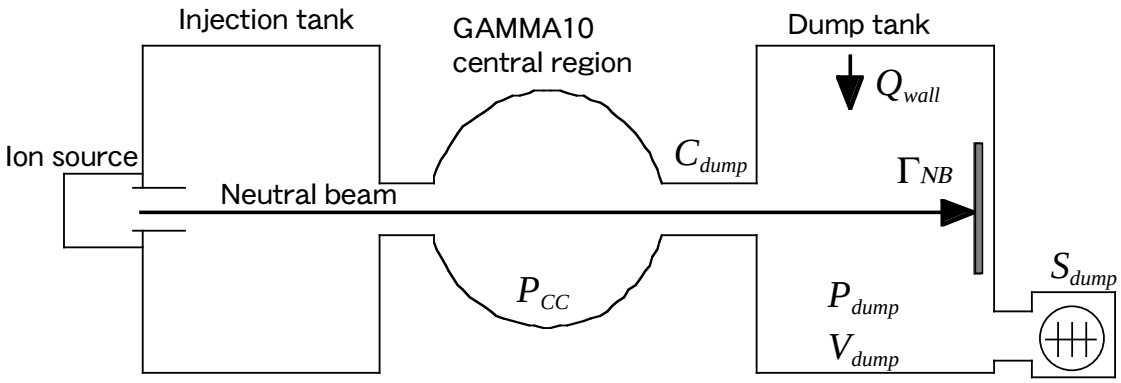

Fig. 5-6 An analytical model for pumping efficiency of CSPBD on the basis of pressure balance equation.

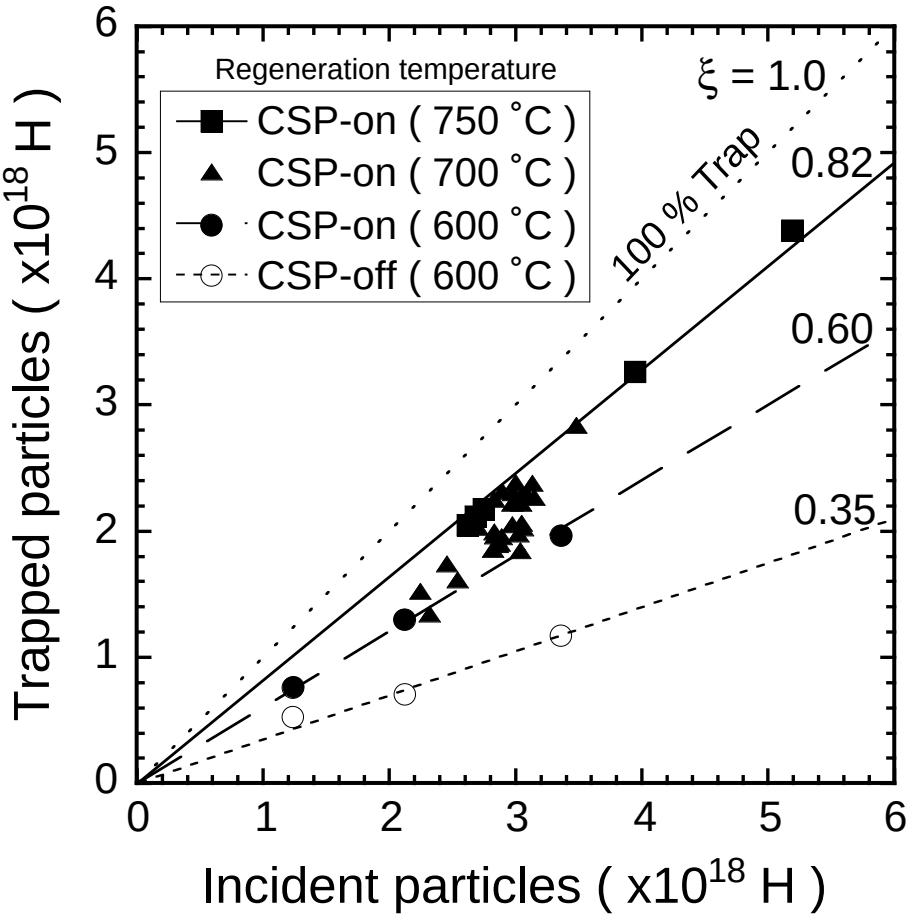

Fig. 5-7 The correlation between the number of incident particles and that of trapped ones by CSPBD. The temperatures in parentheses indicate the regeneration ones.

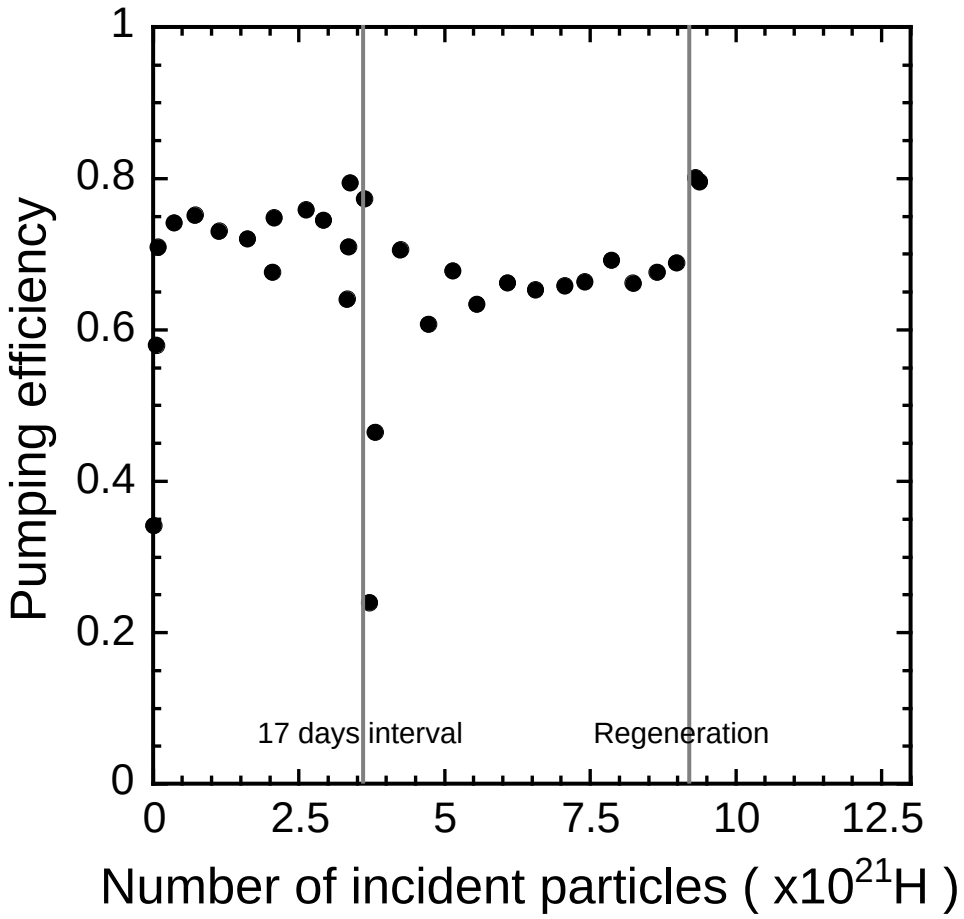

Fig. 5-8 The fluence dependence of the pumping efficiency of CSPBD

6. Feasibility investigation of CSP on GAMMA 10 plasmas

6.1 Objective of this investigation

It has been confirmed from the experimental results and analyses described in the previous chapters that CSP has the pumping effect on the fast neutrals under the condition of the actual device. In this chapter, expectation of the pumping effect on the GAMMA 10 plasmas is described. As previously mentioned, C-NBI system is installed into the central cell for the sake of plasma heating and fueling. However, it is considered that NBI enhances hydrogen recycling in the mid-plane of the central cell, because the major portion of the deposited beam is considered to be trapped by charge-exchange reaction between the energy of beam (~25 keV) and in temperature (T_i ~ a few keV). Possibly due to this enhanced recycling, the degradation of the diamagnetism of the central cell is observed even during the injection. In order to examine whether the application of CSP can suppress the hydrogen recycling enhanced by NBI, the pumping effect of CSP on the GAMMA10 plasma is predicted by means of a numerical simulation.

6.2 Zero-dimensional particle and power balance model in the central cell

A schematic view of zero-dimensional particle and power balance model in the central cell is shown in Fig. 6-1. In the particle balance analysis, the plasma of the mid-plane is divided into three components. One of the components is a group of hot ions

which have the energy as same as NB. The ions except for hot ions belong to a group of warm ions. The electron density is represented as the sum of the density of hot ions and that of warm ones. Hydrogen particles puffed from GP and recycled from the wall belong to a group of neutrals. In the power balance analysis, the plasma is also divided into three components, hot ions, warm ones and electrons. It is assumed that warm ions and electrons can be expressed as Maxwell distribution. Classical loss mechanisms such as charge exchange, electron drag and slowing down are taken into account [2]. The steady-state plasma of the mid-plane is assumed to be sustained by background particle and power flow from the throat region of the central cell. The time evolution of plasma parameter is calculated during and after NBI into the plasma sustained by the back ground flows. The particle balance of each component is given as follows:

$$\frac{dn_w(t)}{dt} = n_0(t)\left[\alpha n_h(t)\left\{\langle\sigma v\rangle_{pi} + \langle\sigma v\rangle_{cx}\right\} + \alpha_w n_w(t)\langle\sigma v\rangle_{pi} + \alpha_w\left\{n_w(t) + n_h(t)\right\}\langle\sigma v\rangle_{ei}\right] + \frac{n_h(t)}{\tau_{ed}^{hot}} + \frac{n_h(t)}{\tau_{sd}} + S_{bg} - n_w(t)\frac{2r_p I(t)}{qV_p v_b}\langle\sigma v\rangle_{cx} - \frac{n_w(t)}{\tau_{Mw}}, \quad (6\text{-}1)$$

$$\frac{dn_h(t)}{dt} = \frac{2r_p I(t)}{qV_p v_b}\left[\left\{n_w(t) + n_h(t)\right\}\left\{\langle\sigma v\rangle_{pi} + \langle\sigma v\rangle_{ei}\right\} + n_w(t)\langle\sigma v\rangle_{cx}\right] - \alpha n_0(t) n_h(t)\langle\sigma v\rangle_{cx} - \frac{n_h(t)}{\tau_{ed}^{hot}} - \frac{n_h(t)}{\tau_{sd}} - \frac{n_h(t)}{\tau_{Mh}}, \quad (6\text{-}2)$$

$$\frac{dn_0(t)}{dt} = \gamma\frac{2r_p I(t)}{qV_p v_b}\left\{n_w(t) + n_h(t)\right\}\langle\sigma v\rangle_{cx} + (\gamma - 1)n_0(t)\left\{\alpha n_h(t)\langle\sigma v\rangle_{cx} + \alpha_w n_w(t)\langle\sigma v\rangle_{cx}\right\} + \gamma\beta\frac{I(t)}{qV_{cc}} + Q_{is} + Q_{bg} - n_0(t)\left[\alpha n_h(t)\langle\sigma v\rangle_{pi} + \alpha_w n_w(t)\langle\sigma v\rangle_{pi} + \alpha_w\left\{n_w(t) + n_h(t)\right\}\langle\sigma v\rangle_{ei}\right] - \frac{n_0(t)}{\tau_{pump}}, \quad (6\text{-}3)$$

where $n_w(t)$, $n_h(t)$ and $n_0(t)$ are density of warm ions, hot ions and neutrals, respectively. $<\sigma v>_{cx}$, $<\sigma v>_{pi}$, and $<\sigma v>_{ei}$ mean rate coefficient of charge exchange, proton and electron ionization, respectively. τ_{ed}^{hot} and τ_{ed}^{warm} denote the time constant of electron drag

for hot and warm ions, respectively. τ_{sd} is the slowing down time of hot ions. τ_{Mh} and τ_{Mw} are the mirror confinement time of hot and warm ions, respectively. τ_{pump} is the time constant of the pumping system of the central cell (0.33 s). α and α_w are the attenuation factor of neutrals for hot and warm ions, respectively. For simplicity, α and α_w are treated as constant and are independent on time. q is the unit charge. V_p is the volume of the plasma (0.21 m^3) and r_p is the plasma radius (0.15 m). v_b is the velocity of neutral beam. $I(t)$ is the current of neutral beam injected into the plasma. γ is the recycling coefficient of the central cell. S_{bg} is the back ground source from the throat region. Q_{is} and Q_{bg} are gas flow from the ion source and the throat region, respectively. The background flow is decided so as to set the left-hand sides of Eqs. (6-1) and (6-3) on zero at $t = 0$.

Power balance of each component is also expressed as follows:

$$\frac{dW_w(t)}{dt} = Q_{bg}^w + \frac{E_b n_h(t)}{\tau_{sd}} - \alpha W_w(t) n_0(t) \langle \sigma v \rangle_{cx} - \frac{\frac{3}{2} n_w(t)\{T_w(t) - T_e(t)\}}{\tau_{ed}^{warm}} - W_w(t) \frac{2 r_p I(t)}{q V_p v_b} \langle \sigma v \rangle_{cx} - \frac{W_w(t)}{\tau_E^{warm}}, \quad (6\text{-}4)$$

$$\frac{dW_e(t)}{dt} = Q_{bg}^e + \frac{m_e}{m_p + m_e} \frac{2 r_p I(t)}{q V_p v_b} \{n_w(t) + n_h(t)\}\{\langle \sigma v \rangle_{pi} + \langle \sigma v \rangle_{ei}\} E_b + \frac{n_h(t)\left\{E_b - \frac{3}{2} T_e(t)\right\}}{\tau_{ed}^{hot}} + \frac{\frac{3}{2} n_w(t)\{T_w(t) - T_e(t)\}}{\tau_{ed}^{warm}} - \kappa \frac{W_e(t)}{\tau_E^{electron}}, \quad (6\text{-}5)$$

where $W_w(t)$ and $W_e(t)$ denote the energy density of warm ions and electrons, respectively. $T_i(t)$ and $T_e(t)$ are the ion and the electron temperature, respectively. τ_E^{warm} and $\tau_E^{electron}$ are the energy confinement time of warm ion and electron. κ is a kind of fitting parameter. Q_{bg}^w and Q_{bg}^e are the power flow supplied to warm ions and electrons, respectively. These flow are also decided so as to set the left-hand sides of Eqs. (6-4) and (6-5) on zero at $t = 0$. The power balance equation as for hot ions is not necessary

because the product of Eq. (6-2) and incident energy E_b is equivalent to the equation with respect to hot ions. The energy, current and timing of NBI and the initial condition ($n_w(0)$, $n_h(0)$, $n_0(0)$, $T_i(0)$, $T_e(0)$) are given in order to solve the above simultaneous equations with respect to t.

6.3 Comparison with experimental results

The time evolution of plasma parameter in the NBI experiment is shown in Fig. 6-2. In this experiment, NB is incident into the target plasma sustained by ICRF1, ICRF2 and ICRF3. The line density is increased by ~ 10 % during NBI. The diamagnetism is decreased even during NBI though it is slightly increased just after NBI turns on. A step-like increase of Hα intensity is measured just after NBI. The gradual increase of the intensity is considered to be caused by hydrogen gas flow from the ion source of the C-NBI system.

A calculation result of NB experiment is shown in Fig. 6-3. In this calculation, $n_e(0) = 2 \times 10^{18}$ m^{-3}, $n_h(0) = 0$ m^{-3}, $n_0(0) = 1 \times 10^{15}$ m^{-3}, $T_w(0) = 3000$ eV, $T_e = 60$ eV, $\gamma = 1.21$ are adopted as the initial condition. Although the acceleration voltage and the drain current of NB are ~ 25 keV and ~30 A, $E_b = 17$ keV and $I_b = 42$ A are actually used as mean values in the calculation. This is because the ratio of ion species (H^+, H_2^+ and H_3^+) obtained from Doppler shift of Hα line is taken into account. For convenience, the acceleration voltage and the drain current of NB are used for the parameters of NB. NB is incident into the target plasma from 10 to 40 ms. A 10 % increase of the electron density, the gradual decrease of energy density and the step-like increase of the neutral density qualitatively predict the experimental results shown in the Fig. 6-2. Although the quantitative treatment of the calculation result remains as a matter to be discussed further, this result indicates a qualitative validity of this particle and power balance

model in the present condition.

6.4 Evaluation of the effect on the plasma performance

6.4.1 Dependence of the coverage of CSP

It is necessary to estimate the installation area of CSP in the central cell for the evaluation of the effect of CSP on the plasma performance. There are many ports for diagnostics, heating and pumping in the central cell. The averaged recycling coefficient γ_{eff} is given by:

$$\gamma_{eff} = (1 - \Theta_{CSP})\gamma + \Theta_{CSP}\gamma_{CSP}, \tag{6-6}$$

where Θ_{CSP} denotes the coverage of CSP and γ_{CSP} is the value obtained from Eq. (5-2). In this case, γ and γ_{CSP} are 1.21 and 0.30, respectively.

Figure 6-4 shows the coverage dependence of the plasma parameter. In this simulation, the initial condition except for the recycling coefficient is the same as used in Fig. 6-3. As shown in the figure, the electron and the hot ion density increase with the coverage of CSP. The diamagnetism also increases with the coverage. The increment of the neutral density is considerably suppressed by the application of CSP. It is thought to be caused by the wall pumping effect of CSP. The decrease of the charge exchange loss during NBI is caused by the reduction of the neutral density. As the coverage of CSP increases, the improvement of the plasma parameter (*e.g.* the density buildup of hot ions, increase of the diamagnetism and suppression of loss power) has a tendency to saturate. In fact, the coverage of CSP is estimated to be 37 % of the inner wall area of the mid-plane with exception of the area where CSP cannot be installed. It is considered from the result of the coverage dependence that this value of the coverage (37%) is sufficient for the improvement of plasma parameter.

The calculation using CSP is carried out with the same initial condition except for

γ_{eff}, and the result is shown in Fig. 6-5. γ_{eff} is evaluated to be 0.87 with CSP. As shown in Fig. 6-5 (c), the increment of the neutral density after NBI is reduced by nearly 80% compared with Fig. 6-3. The increase of the energy density is caused by the suppression of charge exchange loss.

Temporal evolution of the warm ion temperature $T_w(t)$ and warm ion conferment time τ_{Mw} in the cases with and without CSP are shown in Fig. 6-6. The warm ion temperature is sustained during NBI in the case with CSP due to the reduction of the charge exchange loss. As a result, the degradation of the confinement time is getting smaller. It is considered that the continuous increase of the electron density during NBI is caused by the longer confinement time. The comparison between with and without CSP suggests that CSP can improve the energy and particle confinement in NBI experiments.

6.4.2 Dependence of the neutral beam current

The NB current dependence of the density buildup is considered from the viewpoint of fueling by NBI. The calculation results of the plasma parameter in the cases with and without CSP are shown in Figs. 6-7 and 6-8. Values of the drain current are 20, 40, 60, 80 and 100 A, respectively. (They are equivalent to 28, 56, 84, 112 and 140 A of the incident current, respectively.) Each increment of the electron, the hot ion and the energy density grows with the current. In each case of n_e and n_w, however the increment with CSP is much lager than without CSP. The increment of neutral density just after NBI is considerably suppressed by the use of CSP. The increment of the charge exchange loss increasing with the NB current is possibly due to buildup of hot ions and neutrals.

In Fig. 6-9, each increment of the electron Δn_e, hot ion Δn_h and the neutral density Δn_0 are plotted as a function of the beam current in the cases with and without CSP. The

maximum value is adopted as for the electron and the hot ion density since the time at which the density reaches its peak is different in the cases with and without CSP. Concerning the neutral density, the value just after the termination of NBI is adopted in order to remove the influence of the gas flow from the ion source. Δn_e, Δn_h and Δn_0 are proportional with the NB current. Δn_0 is suppressed by CSP as shown in Fig. 6-9 (c). It is clear that the reduction of hydrogen recycling by means of CSP has a beneficial effect on the density buildup of the plasma.

Figure 6-10 (a) shows the time evolution of the density ratio of with to without CSP at the same time. Although the ratio of the electron density is slightly below unity just after the injection, it increases with time. This decrease of the electron density ratio is considered to be caused by the change of the source term owing to the difference of Δn_0 between the cases with and without CSP. Δn_e is proportional to the beam current in the case with CSP as shown in Fig. 6-9 (a). The electron density below 40A of the beam current decreases even during NBI, while the electron density above 60A continues to increase during NBI in the case without CSP (Fig. 6-7 (a)). Thus, the electron density ratio shows a tendency to reach a certain value as the increase of the NB current.

As shown in Fig. 6-10 (b), the density ratio of the hot ion increases with time. However, the density ratio is convex downward below 40 A, while the ratio is convex upward above 60A. Δn_h is proportional to the beam current in the case with CSP as shown in Fig. 6-8 (b). The hot ion density below 40A decreases even during NBI, while the hot ion density above 60A continues to increase during NBI in the case without CSP. The time behavior of the density ratio is caused by that of the hot ion density without CSP.

The ratio of the hot ion density is larger than that of the electron density under the condition of the same time and beam current. This result suggests that the reduction of hydrogen recycling has a significant effect on buildup of hot ions rather than warm ones.

As to the electron density, larger current enhances the density buildup. Finally, results obtained from this simulation suggest that reduction of hydrogen recycling by using CSP makes the density buildup by NBI more effective.

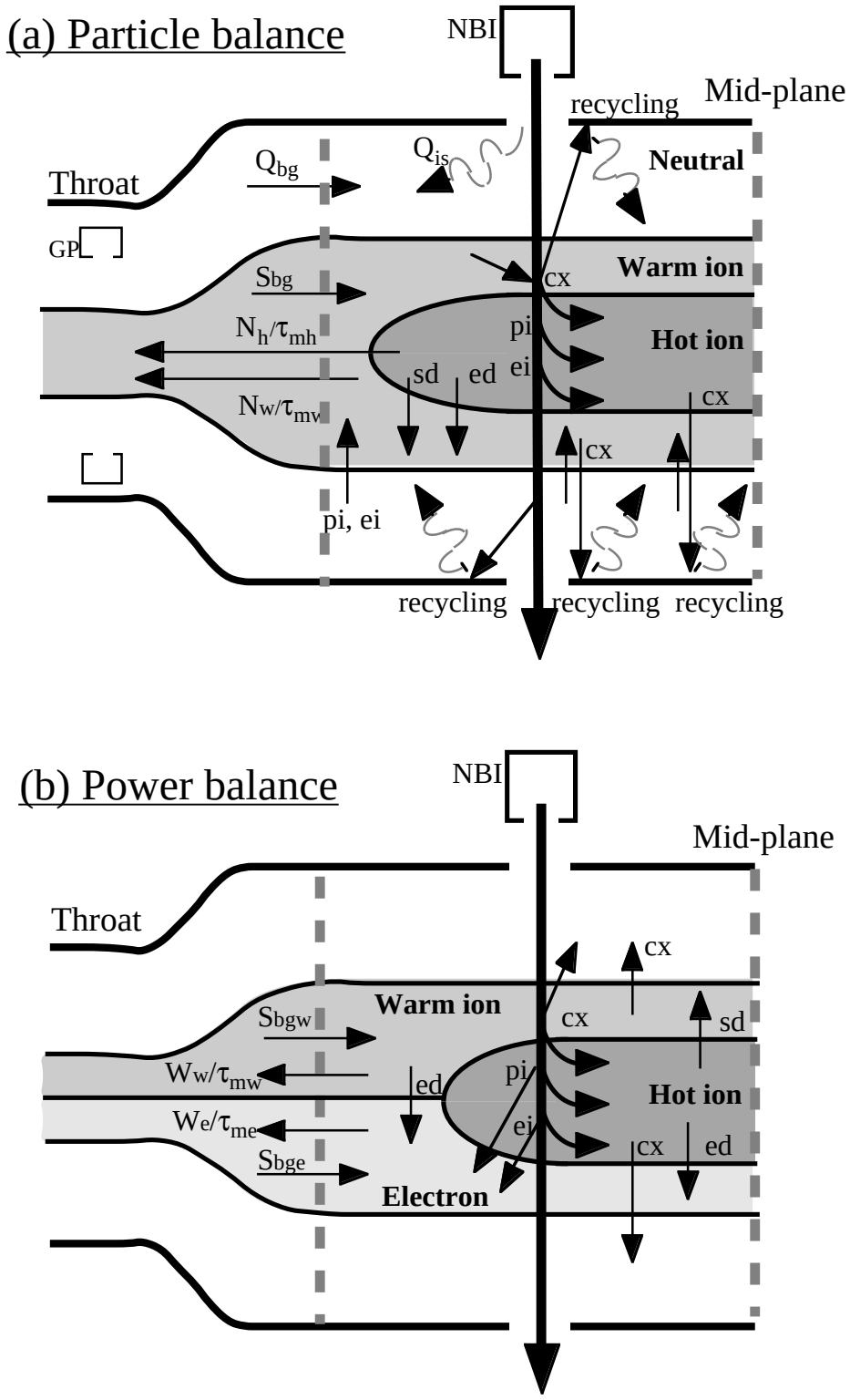

Fig. 6-1 A schematic view of calculation model. (a) particle balance and (b) power balance. cx: charge exchange, pi: proton ionization, ei: electron ionization, ed: electron drag, sd: slowing down.

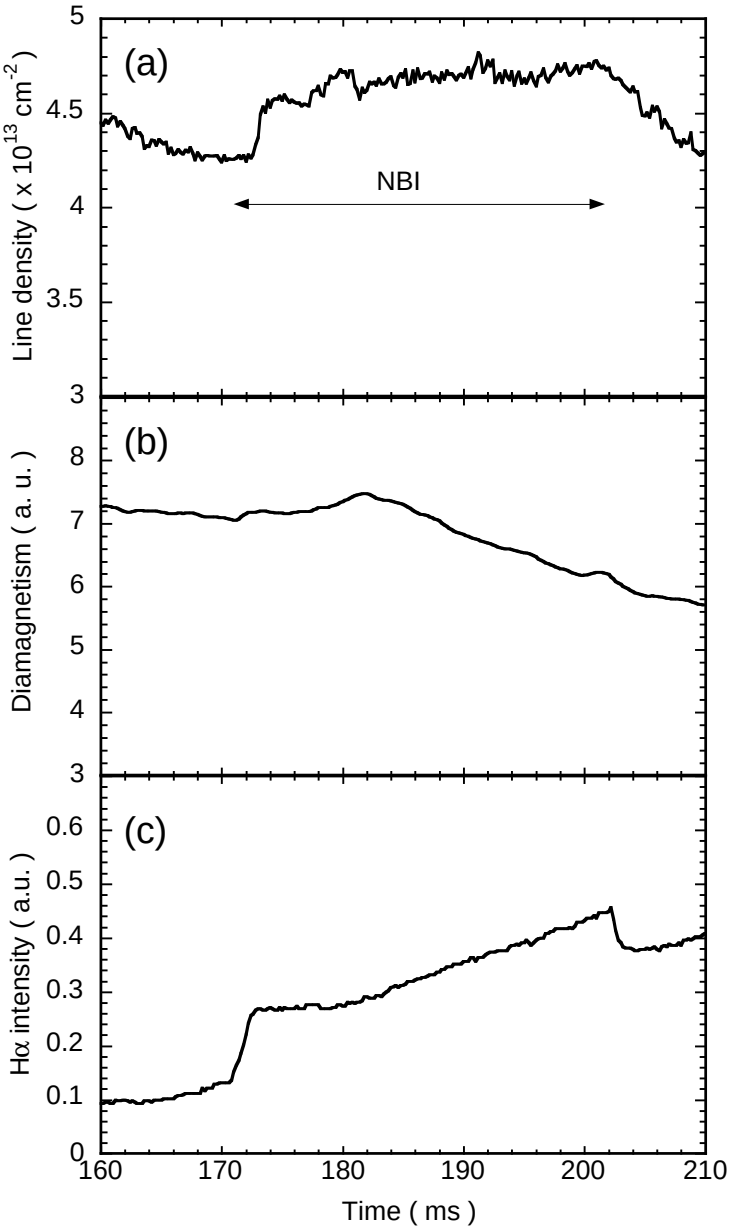

Fig. 6-2 Waveforms of NBI experiment where NB is incident into the plasma sustained by ICRF heating. (a) Electron line density, (b) diamagnetism, (c) Hα line intensity.

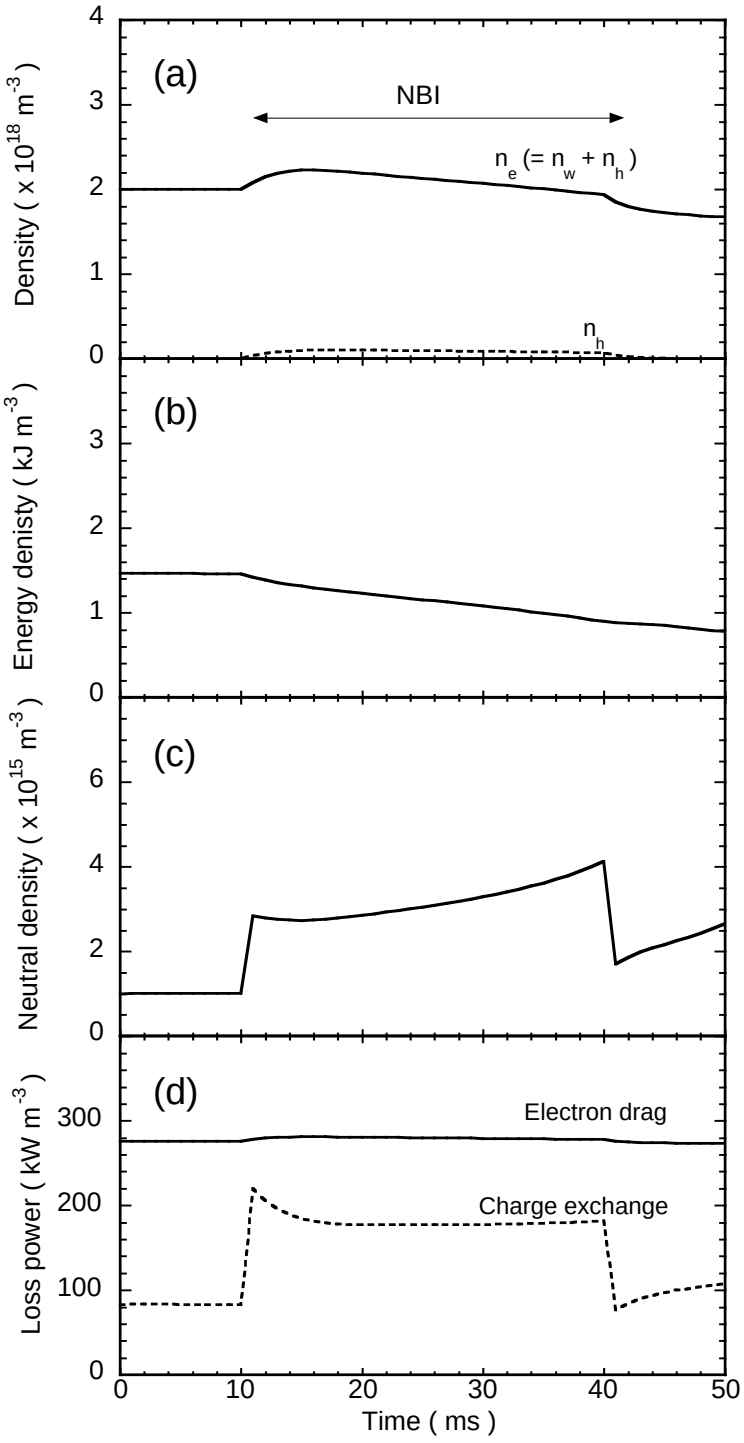

Fig. 6-3 Calculation result of the NB experiment.(a) Electron and hot ion density, (b) energy density, (c) neutral density and (d) loss power caused by electron drag and charge exchange.

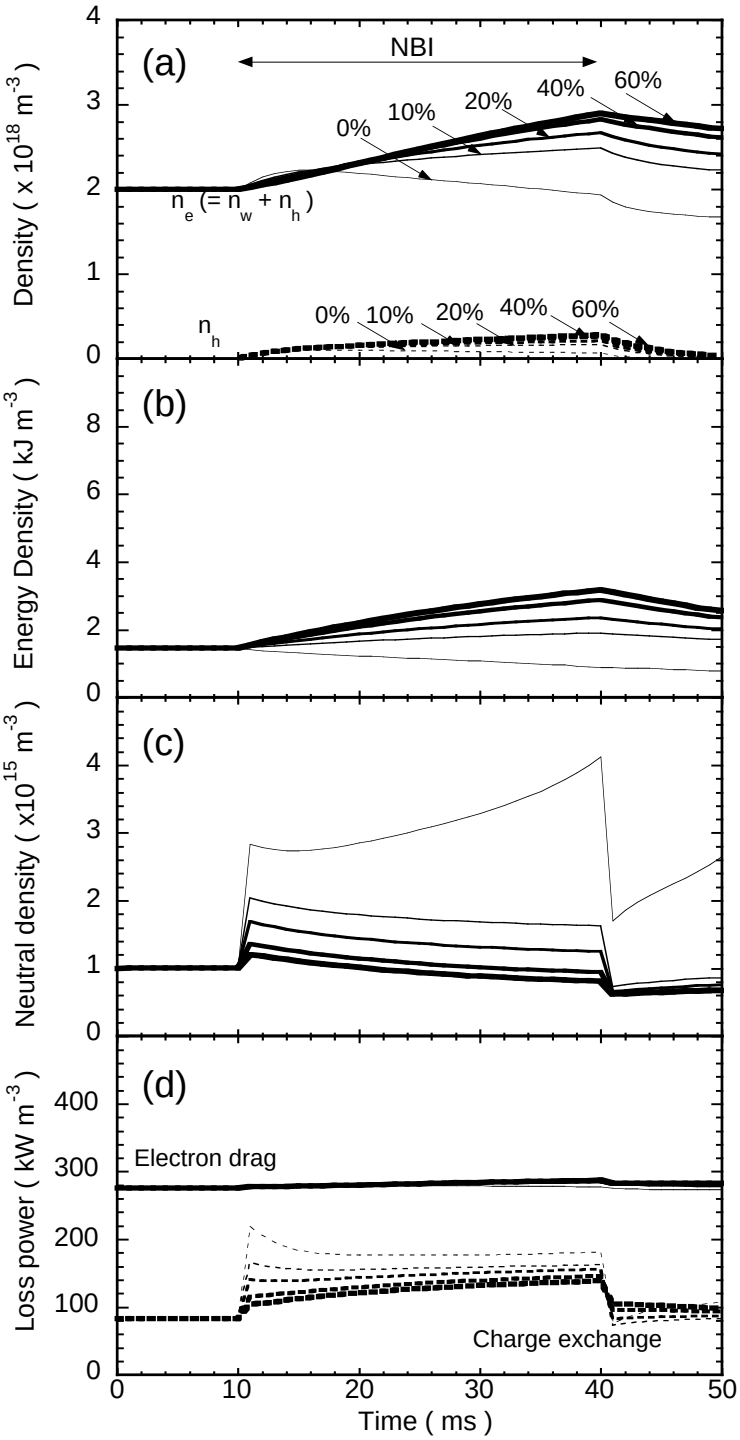

Fig. 6-4 Coverage dependence of plasma parameter. (a) Electron and hot ion density, (b) energy density, (c) neutral density and (d) loss power caused by electron drag and charge exchange.

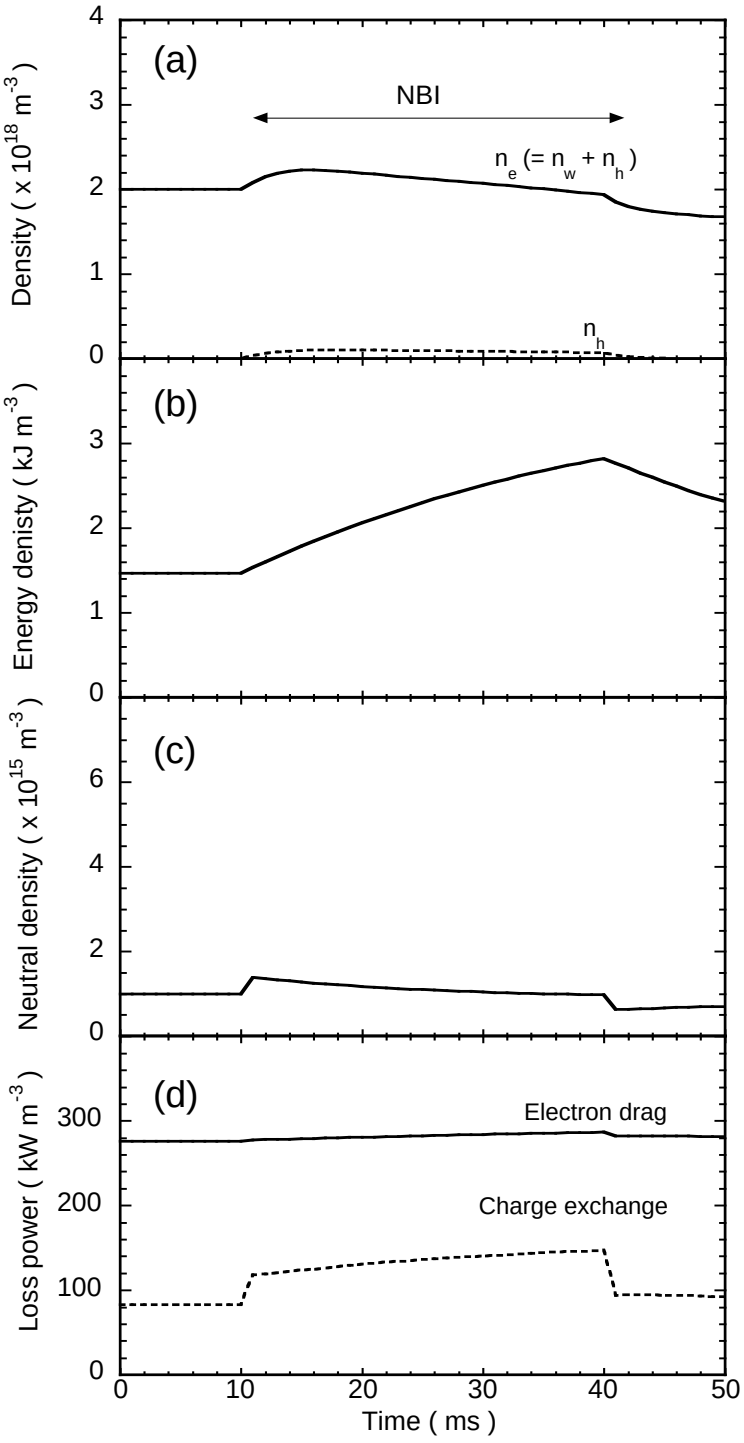

Fig. 6-5 Calculation result of the NB experiment in the case where CSP is installed into 37% of the inner wall area of the mid-plane.

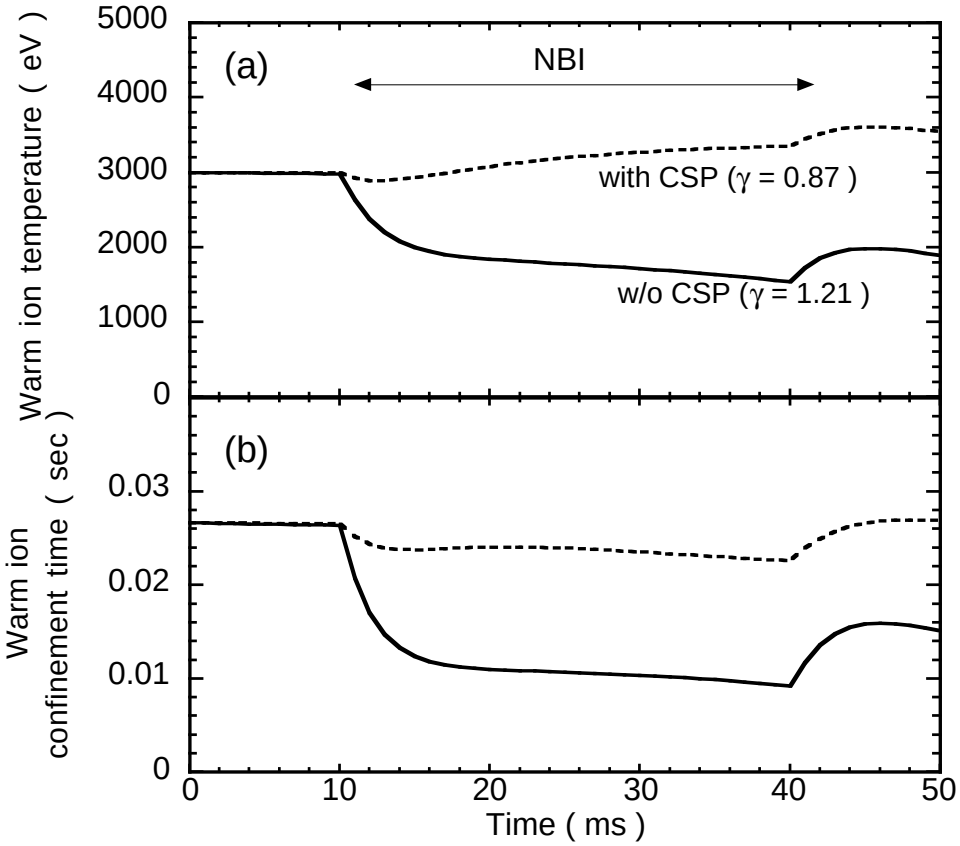

Fig. 6-6 Comparison of the warm ion temperature and the warm ion confinement time between in the cases with and w/o CSP.

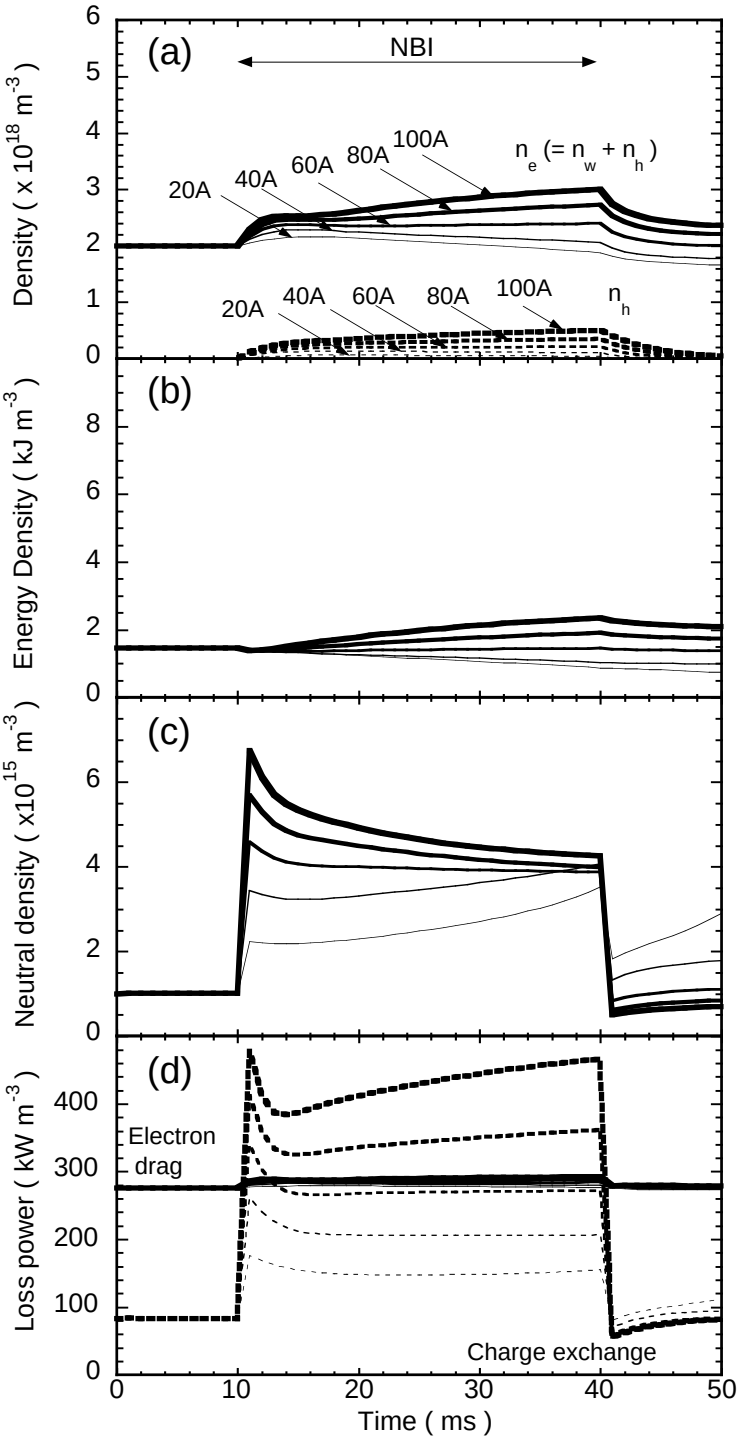

Fig. 6-7 Current dependence of plasma parameters in the case without CSP. (a) Electron and hot ion density, (b) energy density, (c) neutral density and (d) loss power caused by electron drag and charge exchange. The current of NB are 20, 40, 60, 80 and 100 A, respectively.

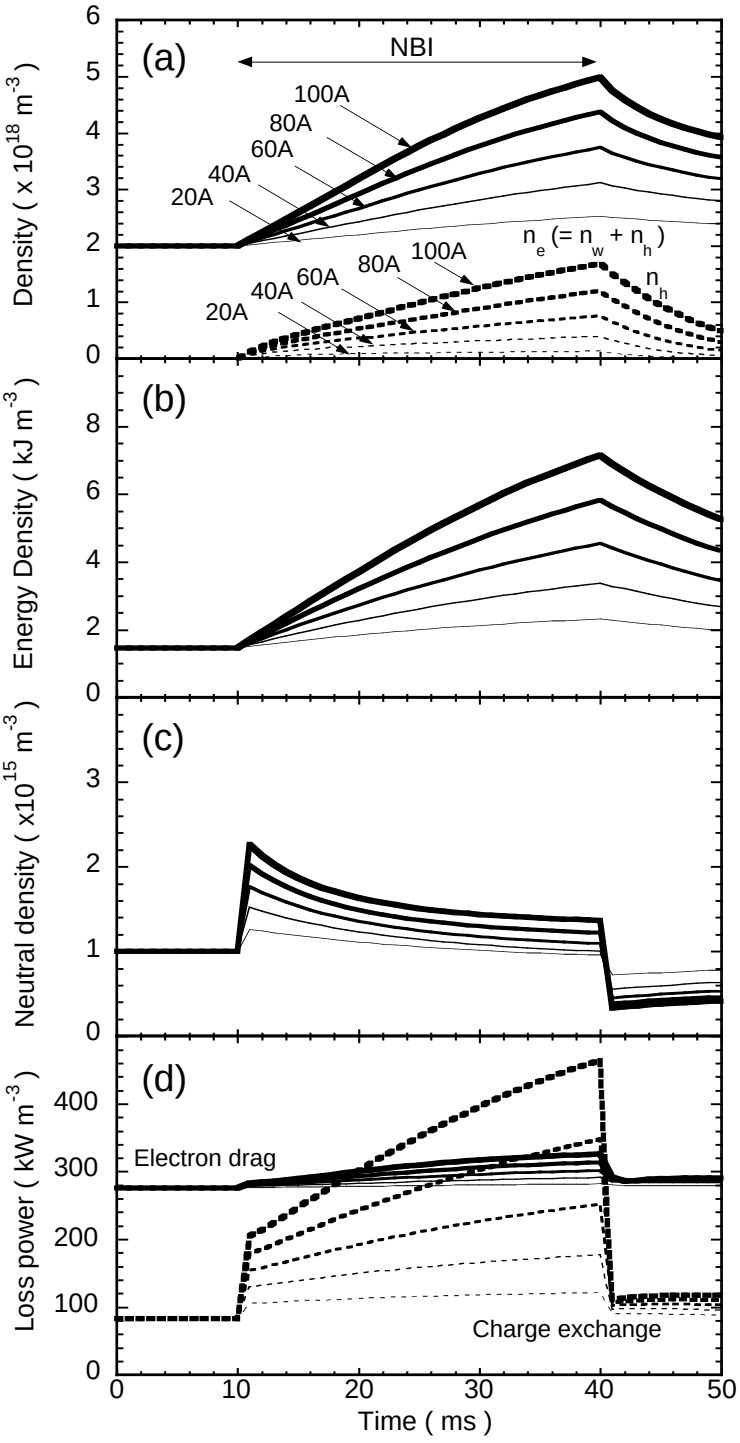

Fig. 6-8 Current dependence of plasma parameter in the case with CSP. (a) Electron and hot ion density, (b) energy density, (c) neutral density and (d) loss power caused by electron drag and charge exchange. The current of NB are 20, 40, 60, 80 and 100 A, respectively.

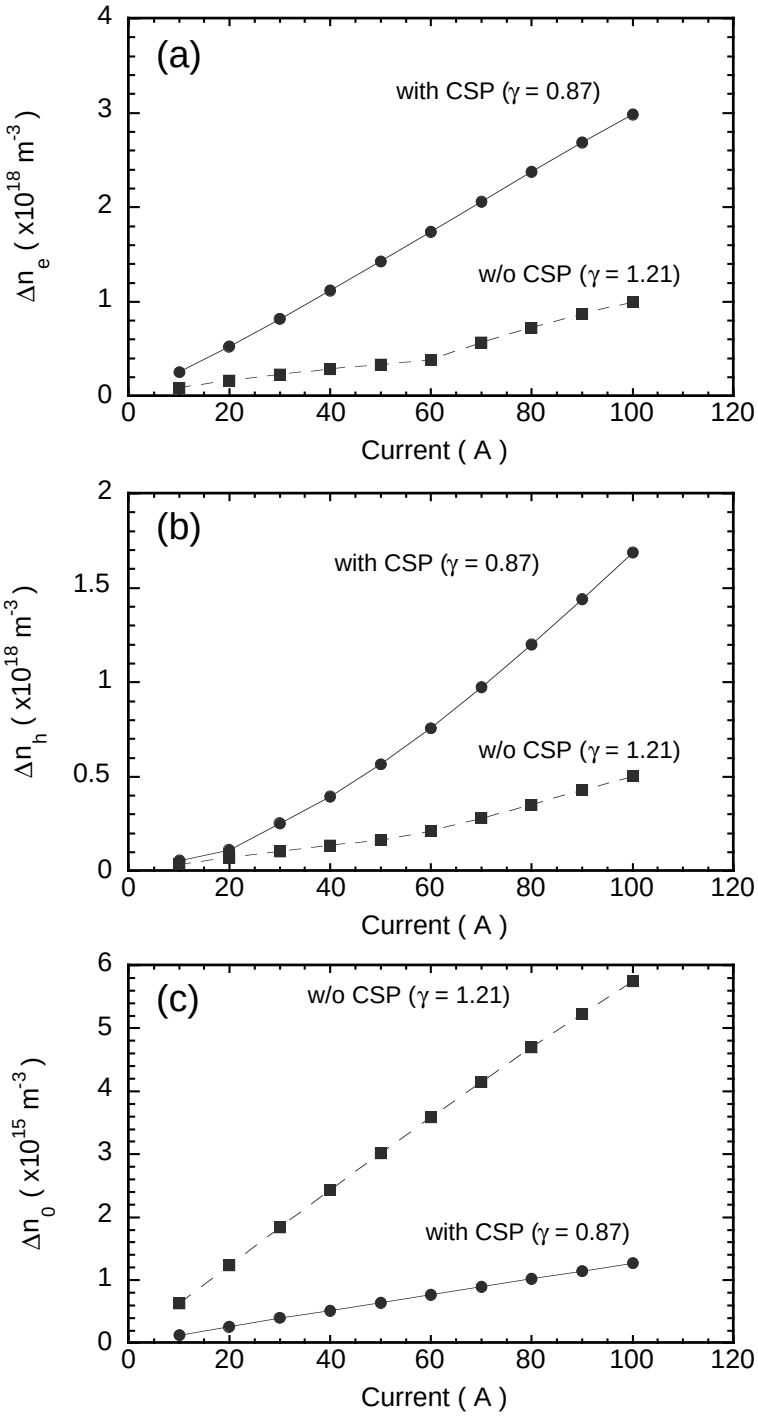

Fig. 6-9 Current dependence of the density increment of (a) the electron and (b) the hot ion and (c) the neutral density in the cases with and w/o CSP.

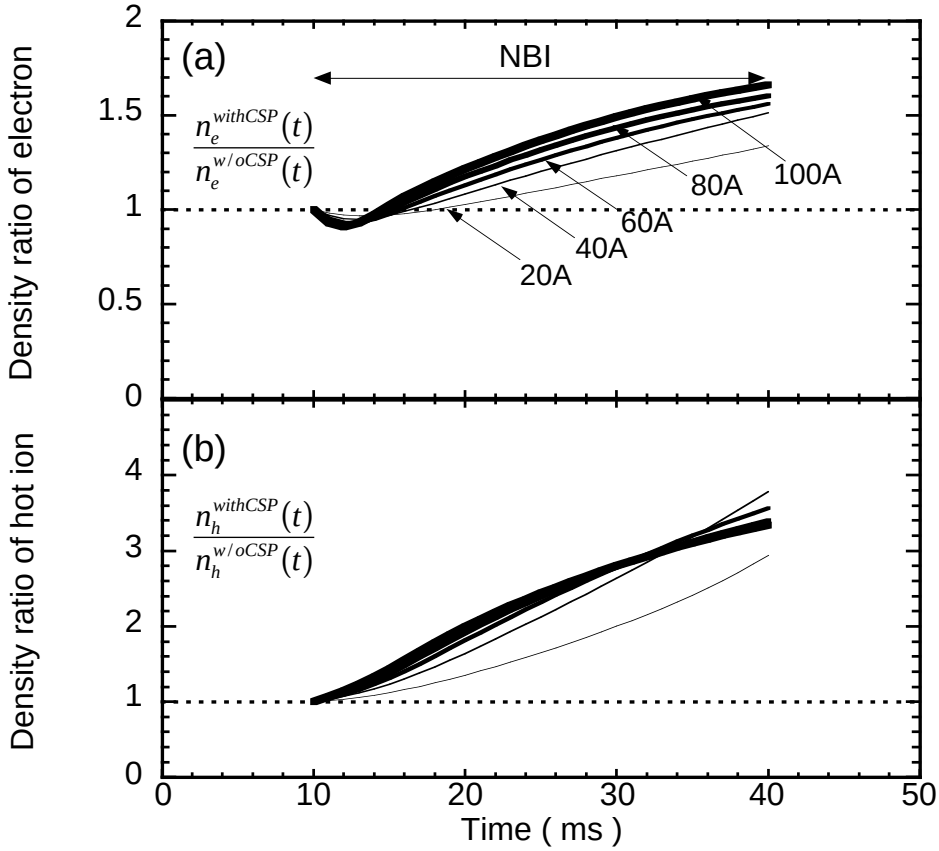

Fig. 6-10 Time evolution of density ratio of (a) electron and (b) hot ion. NB current are 20, 40, 60, 80 and 100 A, respectively.

7. Conclusion

The results obtained in this thesis are described as follows:

A. Pumping effect of CSP on fast neutrals in the test module

The CSP test module, in which a carbon sheet of 170 mm in diameter is mounted, is designed and fabricated in order to investigate the characteristics of pumping effect of CSP. It is confirmed from the pressure difference between CSP-on and -off that CSP has an appreciable pumping effect on the fast neutrals emitted from the GAMMA 10 plasmas. In order to reduce the amount of the adsorbed gas molecule on the CSP surface, pumping experiments are conducted in the temperature range from RT to 250 ˚C. It is found that the amount of water molecule can be decreased at 250 ˚C by 70% compared with the case of RT. The analysis model on the basis of pressure balance equation is proposed in order to estimate the pumping efficiency of CSP. The pumping efficiencies ξ of CSP are estimated to be 0.65 and 0.66 for the cases of 30 ˚C and 200 ˚C, respectively. There is no remarkable difference between two operational temperatures within the experimental error. The method, which reduces adsorbed gases on the CSP surface with sustaining a sufficient pumping efficiency, is established in case that CSP is used in actual plasma conditions.

B. Surface analysis of CFC materials exposed to the GAMMA 10 plasma

Samples of CSP have been analyzed by means of ERD and RBS techniques for the sake of improvement of CSP performance. It has been confirmed that fast neutrals emitted from an actual plasma are trapped in CSP by making a comparison between the hydrogen depth profile of the exposed C/C sample and that of the annealed one. The

hydrogen depth profile of fast neutrals has been roughly explained by the result of Maxwell-distributed ion irradiation by use of the Monte Carlo simulation code TRIM. A minute amount of oxygen (< 1 %) has been detected on the surface of the exposed sample. However, no serious problem probably occurs for the pumping performance of CSP because the analysis was conducted after ventilation and the quantity of oxygen is significantly smaller compared with that of carbon.

C. Application of CSP under the condition of high heat and particle load

CSP is newly applied to the shine-through beam dump of the GAMMA 10 central cell NBI system in order to examine the pumping characteristic of CSP under the condition of high heat and particle load. The result of heat transfer calculation shows that CSP can be used under the present experimental condition by the use of high heat conductive materials. The CSP beam dump is constructed on the basis of the thermal design. Pressure measurements during NBI and the numerical calculation of pressure balance clarified that the number of particles trapped by CSP is proportional to that of incident ones in the pumping experiment. It is confirmed that the pumping efficiency is improved to be 0.82 by adjusting the regeneration temperature to 750 ˚C. It is also found the recovery of the pumping efficiency by regeneration. These results indicate the applicability of CSP under the condition of high heat and particle load.

D. Feasibility study of CSP on the GAMMA 10 plasmas

In order to examine whether the application of CSP can suppress the hydrogen recycling enhanced by NBI, the pumping capability of CSP on the GAMMA10 plasma is evaluated by means of numerical simulation. A zero-dimensional particle and power balance model in the central cell is proposed. The model can qualitatively explain the present NBI experiment. The estimated coverage of CSP (37 %) reduces the increment

of the neutral density just after NBI by nearly 80 %. The comparison between with and without CSP also suggests that CSP can improve the energy and particle confinement in NBI experiments. Results of the current dependence calculation suggest that reduction of hydrogen recycling by using CSP makes the density buildup by NBI more effective.

These results have clarified the characteristics of CSP for reduction of hydrogen recycling. It is considered that they can contribute to improve the plasma performance.

Acknowledgements

The author would like to express his heartfelt gratitude to Prof. K. Yatsu for his continuous guidance and encouragement in the course of the present study. He is sincerely grateful to Prof. Y. Nakashima for his continuous encouragement and significant suggestion in the course of the present study. Their valuable discussions and helpful comments are essential for the accomplishment of the present study.

He wishes to acknowledge helpful comments with Prof. Y. Ootsuka. He also would like to thank Prof. A. Itakura for valuable advice.

He is indebted to Prof. A. Sagara of National Institute for Fusion Science for the invention of CSP and helpful discussions. He also wishes to acknowledge the usage of the Monte Carlo simulation code TRIM with Dr. W. Eckstein of Max-Planck-Institut für Plasmaphysik. He thanks Prof. K. Morita and Dr. J. Yuhara of Nagoya University for the surface analysis of CSP samples. This study is partly performed with the support and under the auspices of the NIFS Collaborative Research Program.

He especially thanks members of Plasma Research Center, University of Tsukuba for their collaboration and support in the experiment.

Finally, he would like to show his gratitude to his mother and brothers for their heartfelt support.

References

[1] G. L. Jackson et al., J. Nucl. Mater. **162-164** (1989) 489.

[2] M. Shoji, Ph. D. thesis University of Tsukuba (1995).

[3] G. Vlases, et al. Nucl. Fusion **27** (1987) 351.

[4] P. A. Pincosy and W. C. Turner, Rev. Sci. Instr. **58** (1987) 1576.

[5] W. Ott et al., Nucl. Fusion **42** (2002) 796.

[6] Y. Nakashima et al., J. Nucl. Mater. (2003) in press (Proceedings of PSI15).

[7] J. Winter, Plasma Phys. Control. Fusion **38** (1996) 1503.

[8] H. F. Dylla et al., Nuclear Fusion **27** (1987) 1221.

[9] H. F. Dylla et al., J. Nucl. Mater. **128-129** (1984) 861.

[10] S. L. Allen et al., J. Vac. Sci. Tech. **A1** (1983) 916.

[11] Y. Sakamoto et al., J. Vac. Soc. Jpn. **32** (1989) 26 (in japanese).

[12] G. M. McCracken, *Tokamaks 2nd ed.* (Ed. J. Wesson, 1996, Clarendon Press, Oxford) 450.

[13] R. A. Conn, Fusion Eng. Des. **14** (1991) 81.

[14] K. Yatsu et al., Nucl. Fusion **41** (2001) 613.

[15] Y. Okamoto, Ph. D. thesis University of Tsukuba (2001).

[16] S. A. Cohen et al., Plasma Phys. Controlled Fusion, **29** (1987) 1205-1217

[17] J. Winter, J. Vac. Sci. Technol. **A5** (1987) 2286.

[18] A. Sagara et al., J. Nucl. Mater. **220-222** (1995) 627.

[19] H. Suzuki et al., Trans. of Fusion Technol. **27** (1995) 523.

[20] Y. Nakashima et al., J. Nucl. Mater. **266-269** (1999) 901.

[21] Y. Ishimoto et al., J. Plasma Fusion Res. SERIES, **3** (2000) 307.

[22] Y. Ishimoto et al., J. Nucl. Mater. (2003) in press (Proceedings of PSI15).

[23] M. Braun and B. Emmoth, J. Nucl. Mater. **128-129** (1984) 657.

[24] R. A. Causey, J. Nucl. Mater. **162-164** (1989) 151.

[25] K. Morita et al., J. Nucl. Mater. **162-164** (1989) 990.

[26] J. Roth, Nucl. Fusion Special Issue (1984) 72.

[27] A. Y. K. Chen et al., J. Nucl. Mater. **227** (1995) 66.

[28] J. Roth, J. Nucl. Mater. **266-269** (1999) 51.

[29] Y. Ishimoto et al., Fusion Eng. Des. Special Issue (2003) in press.

[30] Y. Nakashima et al., Vacuum **41** (1990) 1561.

[31] I. H. Hutchinson, *Principles of Plasma Diagnostics* (Cambridge University Press, 1987).

[32] Y. Nakashima et al., Fusion Eng. Des. **34-35** (1997) 555.

[33] Y. Nakashima et al., Rev. Sci. Instrum. **70** (1999) 849.

[34] W. Eckstein and H. Verbeek, Nucl. Fusion Special Issue (1984) 12.

[35] W. Eckstein and H. Verbeek, Max Plank Institut für Plasma physik, IPP - 9/32(1979).

[36] G. Staudenmaier et al., J. Nucl. Mater. **84**, 149 (1979).

[37] A. Miyahara and T. Tanabe, J. Nucl. Mater. **155-157** (1988) 49.

[38] P. A. Redhead, Vacuum **12** (1962) 203.

[39] K. Ashida, J. Nucl. Mater. **128&129** (1984)792.

[40] K. Ashida *et al.*, J. Nucl. Mater. **111&112** (1982) 769.

[41] K. Morita and Y. Muto, J. Nucl. Mater. **196-198** (1992) 963.

[42] D. K. Brice, Nucl. Instr. Meth. **B44** (1990) 302.

[43] W. Möller and B. M. U. Scherzer, Appl. Phys. Lett. **50** (1987) 1870.

[44] Ch. Wild and P. Koidl, Appl. Phys. Lett. **51** (1987) 1506.

[45] B. Tsuchiya and K. Morita, J. Nucl. Mater. **226** (1995) 293.

[46] D. Heifetz et al., J. Comput. Phys. **46**, 309 (1982).

[47] Y. Nakashima et al., J. Nucl. Mater. **241-243**, 1011(1997).

[48] K. Morita and Y. Muto, J. Nucl. Mater. **220-222** (1995) 1038.

[49] K. Morita et al, J. Nucl. Mater. (2003) in press (Proceedings of PSI15)

[50] K. Morita, *Private communication.*

[51] L. C. Feldman and J. W. Mayer, *Fundamentals of Surface and Thin Film Analysis* (Elsevier Science Publishing, 1986).

[52] K. Morita et al., J. Nucl. Mater. **248** (1997) 27.

[53] J. H. Foote et al., Rev. Sci. Instrum. **54** (1983) 928.

[54] J. F. Ziegler, J.P. Biersack and U. Littmark, *The Stopping and Range of Ions in Solids* (Ed. J. F. Ziegler, Vol. 1 of The Stopping and Ranges of Ions in Matter, Pergamon Press, 1985).

[55] H. H. Andersen, *Hydrogen Stopping Powers and Ranges in All Elements* (Ed. J. F. Ziegler, Vol. 3 of The Stopping and Ranges of Ions in Matter, Pergamon Press, 1977).

[56] J. F. Ziegler, *Helium Stopping Powers and Ranges in All Elemental Matter* (Ed. J. F. Ziegler, Vol. 4 of The Stopping and Ranges of Ions in Matter, Pergamon Press, 1977).

[57] J. F. Ziegler and J.P. Biersack, *SRIM*, Computer software, IBM research, 2000. (The latest version of *SRIM* is available at "http://www.srim.org/".)

[58] W. Eckstein, *Computer Simulation of Ion-solid Interaction*, Springer, Berlin, 1991.

[59] J.P. Biersack and L. G. Haggmark, Nucl. Instrum. Methods. **174** (1980) 257.

[60] J.P. Biersack and W. Eckstein, Appl. Phys. 34 (1984) **73**.

[61] M. Ulrickson, The JET Team and The TFTR Team, J. Nucl. Mater. **176-177** (1990) 44.